Hippocampal-prefrontal theta coupling develops as mice become proficient in associative odorant discrimination learning

Daniel Ramirez-Gordillo[1], Andrew A. Parra[1], K. Ulrich Bayer[2,3] and Diego Restrepo[1,2,#]

[1]Department of Cell and Developmental Biology, University of Colorado Anschutz Medical Campus, Aurora, CO 80045, USA

[2]Program in Neuroscience, University of Colorado Anschutz Medical Campus, Aurora, CO 80045, USA

[3]Department of Pharmacology, University of Colorado Anschutz Medical Campus, Aurora, CO 80045, USA

[#]Corresponding author: Diego Restrepo, diego.restrepo@cuanschutz.edu

Abstract

Learning and memory requires coordinated activity between different regions of the brain. Here we studied the interaction between medial prefrontal cortex (mPFC) and hippocampal dorsal CA1 during associative odorant discrimination learning in the mouse. We found that as the animal learns to discriminate odorants in a go-no go task the coupling of high frequency neural oscillations to the phase of theta oscillations (phase-amplitude coupling or PAC) changes in a manner that results in divergence between rewarded and unrewarded odorant-elicited changes in the theta-phase referenced power (tPRP) for beta and gamma oscillations. In addition, in the proficient animal there was a decrease in the coordinated oscillatory activity between CA1 and mPFC in the presence of the unrewarded odorant. Furthermore, the changes in PAC resulted in a marked increase in the accuracy for decoding odorant identity from tPRP when the animal became proficient. Finally, we studied the role of Ca^{2+}/calmodulin-dependent protein kinase II α (CaMKIIα), a protein involved in learning and memory, in oscillatory neural processing in this task. We find that the accuracy for decoding the odorant identity from tPRP decreases in CaMKIIα knockout mice and that this accuracy correlates with behavioral performance. These results implicate a role for PAC and CaMKIIα in olfactory go-no go associative learning in the hippocampal-prefrontal circuit.

Introduction

Learning and memory are two crucial abilities important for survival of organisms (Klein et al., 2002). Our lives are enhanced, and our personalities are shaped due to the ability to learn and form memories. Therefore, it is not surprising that often diseases that affect these abilities are devastating and frequently the individual affected becomes dependent on others. Learning and memory requires coordinate activity between different regions of the brain (Colgin, 2011; Gordon, 2011; Headley and Paré, 2017; Lisman et al., 2017). Local field potential oscillations reflect activity of temporally coordinated neuronal groups providing a reference for spike timing-based codes and gating information transfer between distant brain regions. In phase amplitude coupling (PAC), the amplitude of the bursts of a faster oscillation is larger within a phase window of a slower carrier wave (Tort et al., 2010). In a previous publication, we characterized PAC in the olfactory bulb of mice learning to discriminate odorants in a go-no go associative learning task and we introduced a measure of the magnitude of phase-locked high gamma and beta bursts as a function of time: the theta phase-referenced power (tPRP). We found that PAC changes throughout learning and that odorant-elicited changes in tPRP increase for rewarded and decrease for unrewarded odorants in the proficient mouse (Losacco et al., 2020). Furthermore, we showed that contextual odorant identity (is the odorant rewarded?) can be decoded from peak tPRP in animals proficient in odorant discrimination, but not in naïve mice. As the animal learns to discriminate the odorants, the dimensionality of PRP decreased. These findings in the olfactory bulb, the first relay station in the olfactory system, raised the question whether

downstream areas of the brain receiving input from the olfactory bulb experience a similar phenomenon.

In the current study, we assessed decoding of odorant identity from oscillatory neural activity in animals learning to discriminate odorants in the go-no go task in two downstream brain areas of the brain that receive input from the olfactory bulb: the dorsal cornu ammonis area 1 (CA1) area of the hippocampus and medial prefrontal cortex (mPFC). These brain areas are involved in learning of odorant valence and attention to odorants (Cansler et al., 2021; Gourevitch et al., 2010; Li et al., 2017; Martin et al., 2007) and exhibit oscillatory coupling disrupted in animal models of schizophrenia (Colgin, 2011). Additionally, we chose to study decoding in Ca^{2+}/calmodulin-dependent protein kinase II α (CaMKIIα) knockout mice (CaMKIIα KO) because of the essential role of this protein in learning and memory in the hippocampus (Bayer and Schulman, 2019; Bear et al., 2018; Lisman et al., 2012). CaMKIIα plays a role in long term potentiation (LTP) and long-term depression (LTD) and dentate gyrus neurogenesis, essential processes for learning and memory (Cook et al., 2021; Coultrap et al., 2014; Malinow et al., 1989; Silva et al., 1992b; Suarez-Pereira et al., 2015). Deficiencies in the function of CaMKIIα have been implicated in a range of diseases including schizophrenia, addiction, depression, epilepsy, and neurodevelopmental disorders (Chia et al., 2018; Robison, 2014). CaMKIIα KO are viable and display impaired spatial memory and reduced LTP in the hippocampus (Silva et al., 1992a; Silva et al., 1992b). Mice heterozygous for CaMKIIα knockout (CaMKIIα Hets) have problems with working memory and increased anxiety, and aggressiveness, characteristic of schizophrenia

(Chen et al., 1994; Hasegawa et al., 2009; Matsuo et al., 2009; Yamasaki et al., 2008). Large genome screens have found significant heterozygous mutations in CaMKIIα in schizophrenia patients (Fromer et al., 2014; Purcell et al., 2014). Furthermore, because of the role of CaMKIIα in development and neurogenesis, CaMKIIα Het mice have an immature dentate gyrus (Yamasaki et al., 2008). The undeveloped brain leads to dysfunctions in the neuronal circuity leading to an altered perception of reality and cognitive dysfunctions (Walton et al., 2012).

We recorded neural activity from both hippocampal dorsal CA1 and mPFC in mice engaged in a go-no go task where they learn to respond to a rewarded odorant and refrain from responding to the unrewarded odorant (Losacco et al., 2020). We surveyed PAC changes throughout learning by calculating the modulation index (MI), a measure of PAC strength, and the variance of peak angle, a measure of the variance of the theta phase for gamma oscillations (Losacco et al., 2020; Tort et al., 2010). We show that the MI and peak angle variance change as the animal becomes proficient and we find a difference in these measures of PAC between wild type mice (WT) and CaMKIIα knockout (KO) and heterozygous (Het) mice. In addition, the odorant-elicited changes in tPRP decrease for unrewarded odorants as the animal learns and tPRP differs between CaMKIIα KO and WT. Furthermore, the accuracy for decoding contextual odorant identity from tPRP increased as the animal became proficient and this increase was smaller for CaMKIIα KO mice. Finally, we show an increase in the odorant-induced change in coordinated neural activity between CA1 and mPFC as the animal becomes proficient at discriminating between odorants and the odorant-induced change in

106 coordinated neural activity is smaller in CaMKIIα KO mice. These results demonstrate
107 increased decoding accuracy from phase-referenced oscillatory power in CA1 and
108 mPFC as the animal learns to differentiate odorants and a role of CaMKIIα in learning-
109 induced changes in PAC and coordinated oscillatory neural activity between
110 hippocampus and mPFC.
111
112

Results

Dual CA1-mPFC tetrode recording in mice undergoing the go-no go olfactory discriminating task.

The goal of this study was to determine whether changes in coupled oscillations that occur in the olfactory bulb as mice learn to discriminate odorants in a go-no go task are observed in downstream areas of the brain (mPFC and hippocampus). These downstream areas receive input originating from the olfactory bulb and oscillations in the bulb are known to be coupled to the hippocampus and throughout the brain (Martin et al., 2007; Nguyen et al., 2016; Tort et al., 2018). We also wanted to determine whether there was a difference between the CaMKIIα KO, CaMKIIα Hets and the WT mice in PAC and whether the peak or trough of the oscillation carries different information allowing the mouse to learn to differentiate between a pair of odorants. Lastly, we determined whether coordinated neural activity changed as the animal learned to discriminate odorants and we asked whether there was a difference in the relationship of oscillations between CA1 and mPFC between the different CaMKIIα genotypes. Thirsty mice learned to lick on a spout in the presence of a rewarded odorant (S+) to obtain a water reward and refrained from licking in the presence of unrewarded odorant (S-) in a go-no go associative learning task (Losacco et al., 2020). The odorants were presented in pseudorandomized order in the go no-go task (Figure 1A–D). The odorant pairs tested were different volatile compounds (Table 1) and we found no difference in any measurements between odorant pairs.

In the go-no-go odorant discrimination task, mice start the trial at will by licking on the lick port. The odorant is delivered at a random time 1–1.5 s after nose poke (the time course for the trial is shown in Figure 1C). The mice learn to either lick a waterspout at least once during each 0.5 s segment in the 2 s response area to obtain a water reward for the rewarded odorant or refrain from licking for the unrewarded odorant. Mice refrain from licking during presentation of the unrewarded odorant because of the effort it takes to lick. Behavioral performance was termed naïve or proficient when their performance estimated in a 20-trial window was below 65% for naïve and above 80% for proficient. Mice were trained in the task for sessions of up to 200 trails. In the last session training ended after the animal achieved two 20-trial blocks of proficient performance; valence was reversed the next day or another odorant was tested. We recorded the LFP using 2 tetrodes (4 electrodes per tetrode) implanted in the CA1 of the hippocampus and 2 tetrodes in ipsilateral mPFC, and we analyzed the data to determine whether the different genotypes differ in cross-frequency coupling for naïve or proficient mice (Figure 1E). The dataset is comprised of 747 recording sessions in 18 mice. The odorant pairs tested were different volatile compounds (or mixtures) whose nomenclature addresses the odorant names and the experimental set (e.g., APEB, see Table 1 for the nomenclature). Table 2 enumerates the total number of sessions per odorant pair, mouse, and experiment.

We performed PAC analysis of the LFP recorded in the go no-go behavioral task. PAC analysis is a cross-frequency coupling analysis to determine whether high frequency

159 oscillation bursts take place at specific phases of low frequency theta oscillations (Tort
160 et al., 2010). PAC has been reported in brain areas such as the olfactory bulb,
161 hippocampus and prefrontal cortex (Belluscio et al., 2012; Colgin, 2015; Kaplan et al.,
162 2014; Losacco et al., 2020; Rojas-Libano et al., 2014; Scheffer-Teixeira and Tort, 2016).
163 Figures 1E i–iv show an example of high gamma/theta PAC for the LFP recorded in
164 CA1. Figure 1E i shows the extracellular LFP sampled for hippocampus at 20 kHz and
165 filtered between 1–750 Hz. The raw signal (Figure 1 E i) was filtered with a 20th order
166 Butterworth filter into different LFP frequency bands (Figures 1E ii, iii, iv) (theta, 6–14
167 Hz, adapted from (Nguyen Chi et al., 2016) high gamma, 65–95 Hz). We used PAC
168 analysis (Tort et al., 2010) to evaluate the degree of coupling of the amplitude of the
169 envelope of the beta or high gamma LFP on the phase of the theta LFP. Figure 1E iii
170 shows the theta phase and in Figure 1 E iv shows the envelope for the amplitude of the
171 high gamma LFP, both calculated with the Hilbert transform as detailed in Tort et al.
172 (2010). Figures 1 E ii and iv show that the filtered high gamma LFP changes amplitude
173 in manner that appears coordinated with the theta phase.
174
175 **The peak angle variance of PAC increased for the unrewarded odorant as the**
176 **animals became proficient differentiating between odorants**
177
178 We proceeded to ask whether the strength of PAC, quantified by the modulation index
179 (MI), changes as the animal learns to differentiate odorants in the go-no go task. MI is a
180 measure of how localized high frequency firing is within the phase of theta oscillations
181 (Tort et al 2010). Figures 2A–C illustrate an example of high gamma tPAC for S+ and S-

odorant trials in two sessions for naïve and proficient mice. The phase amplitude plots for the trials are shown in pseudocolor in Figure 2A, for a WT mouse during the naïve (2Ai-iii) and proficient (2Aii-iv) stages and the percent correct as a function of trial number is shown for the two sessions in Figure 2B. In this example there appears to be an increase in the strength of PAC when the animal becomes proficient differentiating between the odorants. Furthermore, there was an increase in peak angle variance for the unrewarded odorant as shown by the peak angle polar histograms in Figures 2C i, ii. Figure 2C i shows that for the unrewarded odorant the peak angle was near 90 degrees during the naïve stage while Figure 2C ii shows the peak angle for the unrewarded odorant fluctuated widely during the proficient stage. This is in contrast with the rewarded odorant for which the peak angle remained near 90 degrees during naïve (Figure 2C iii) and proficient stages (Figure 2C iv).

Figure 2D shows the differences in MI computed per mouse, per odorant pair between S+ and S- for naïve and proficient mice for tPAC for hippocampus (i) beta (ii) high gamma and mPFC (iii) beta (iv) high gamma. For the beta tPAC MI for both the hippocampus and mPFC a generalized linear model (GLM) analysis finds statistically significant differences between S+ vs. S- and the interaction between S+ vs. S- and naïve vs. proficient ($p<0.001$, 188 observations, 184 d.f., F-statistic=51,67.7, $p<0.001$, 6 mice, 8 odor pairs, Supplementary Table 1). GLM does not find significant differences for MI for high gamma tPAC ($p>0.05$). Figure 2E shows differences for peak angle variance between S+ and S- for naïve and proficient mice for hippocampus tPAC (i) for beta and (ii) high gamma and for mPFC tPAC for (iii) beta and (iv) high gamma. For

both beta and gamma tPAC and for both the hippocampus and mPFC GLM finds statistically significant differences between S+ vs. S- and the interaction between S+ vs. S- and naïve vs. proficient ($p<0.001$, 188 observations, 184 d.f., F-statistic=19.5-26.4, $p<0.001$, 6 mice, 8 odor pairs, Supplementary Table 2) and for naïve vs. proficient ($p<0.05$). Asterisks in all figures show pairwise statistical significance (t test or ranksum test, p< pFDR, p value for significance corrected for multiple comparisons using the false discovery rate (Curran-Everett, 2000)).

Overall, we found an increase in peak angle variance for the unrewarded odorant as the animal became proficient. We also found small, but significant changes in the strength of beta tPAC that differed between the S+ and S- odorants as the animal learned to discriminate odorants.

The odorant-elicited change in the theta phase-referenced beta and gamma power became negative for the unrewarded odorant as the mice became proficient discriminating between odorants

Wavelet power referenced to theta phase (peak or trough) was determined to evaluate whether it changes as the animal learns. This analysis is referred to as theta phase-referenced power (tPRP) (Losacco et al., 2020). Figure 3A shows examples of the time course during the trial for the average wavelet broadband LFP spectrograms for 30 trials during naïve S+ (i), 27 trials during naïve S- (ii) 84 trials during proficient S+ (iii) and 84 trials during proficient S- (iv). After odorant onset there was an increase in

228 broadband power for the S+ odorant and a decrease in power for the S- odorant as the
229 animal became proficient.
230
231 Figure 3B shows the time course during the trial for the average high gamma tPRP
232 referenced to the peak (red) or trough (blue) of theta for the proficient trials in Figure 3A.
233 For the rewarded (S+) odorant the power increased for the peak and decreased for
234 trough after addition of the odorant while for the unrewarded odorant both peak and
235 trough tPRPs decreased. Figure 3C shows that, as expected, there was an increase in
236 the lick rate for the rewarded odorant and a decrease for the unrewarded odorant.
237 Finally, Figures 3D,E show a per mouse per odorant pair analysis that indicated that
238 tPRP became negative for S- as the mice became proficient. E: peak, F: through, (i)
239 beta and (ii) gamma hippocampus (iii) beta and (iv) gamma mPFC. GLM finds
240 statistically significant differences for tPRP between S+ vs. S- and the interaction
241 between S+ vs. S- and naïve vs. proficient ($p<0.001$, 376 observations, 368 d.f., F-
242 statistic=72.7-103, $p<0.001$, 6 mice, 8 odor pairs, Supplementary Table 3).
243
244 In addition, we asked whether odorant-induced changes in peak tPRP changed when
245 odorant valence was reversed. Panels A i and ii of Figure 3 - figure supplement 1 show
246 an example of the time course for the peak (red) and trough (blue) high gamma tPRP
247 when the mouse was proficient for a forward session where the rewarded odorant (S+)
248 was acetophenone (AP) and the unrewarded odorant (S-) was ethyl benzoate (EB).
249 Panels A iii and iv of Figure 3 figure supplement 1 show that when the valence of the
250 odorant was reversed (AP was S- and EB was S+) the response to EB resembled the

response to AP in the forward sessions (compare panels A ii and iv of Figure 3 figure supplement 1) indicating that the response is a response to the contextual identity of the odorant (is it rewarded?) as opposed to the chemical identity of the odorant. Figure 3 figure supplement 1 (B,C) shows a summary bar graph/violin plot analysis per mouse per odorant pair of all reversal experiments indicating that for the proficient mouse the average peak and trough tPRP decreases for the unrewarded S- odorant regardless of the identity of the odorant. For high gamma tPRP GLM finds statistically significant differences for S+ vs. S- and peak vs. trough ($p<0.001$, 188 observations, 180 d.f., F-statistic=61.8, $p<0.001$, 6 mice, 8 odor pairs, Supplementary Table 4) and does not find a difference between forward and reverse sessions indicating that indeed the high gamma tPRP responds to the contextual odorant identity. For beta tPRP GLM finds a statistically significant difference for S+ vs. S- ($p<0.001$, 188 observations, 180 d.f., F-statistic=87, $p<0.001$, 6 mice, 8 odor pairs, Supplementary Table 4) and interestingly, GLM does find a small statistically significant differences between forward vs. reverse ($p<0.05$) for beta tPRP. Although this is a relatively small difference, this indicates that beta tPRP is not exclusively responsive to contextual odorant identity and that these brain regions may also encode information on the chemical identity of the odorant.

The accuracy for decoding the contextual identity of the odorants from theta phase referenced power increased when the mice became proficient

We proceeded to determine whether we could decode contextual odorant identity from tPRP. Decoding was performed using a linear discriminant analysis (LDA) to set a

decision boundary hyper-plane between binary stimulus classes (S+ versus S-) (Vizcay et al., 2015). LDA was trained with tPRP from each electrode for each mouse (8 electrodes in the hippocampus and 8 electrodes in the mPFC per mouse) for all trials except one (the training dataset) and then the tPRP from the missing trial (test data) was classified as S+ or S-. This was done at both naïve and proficient learning stages. As a control we shuffled the identity of trials in the training set.

Figure 4A shows an example of the time course during the trial for the decoding accuracy for one mouse for the LDA trained using CA1 tPRP for the EAPA odor pair for (i) naïve stage beta, (ii) proficient stage beta, (iii) naïve stage gamma, (iv) proficient stage gamma. For the naïve animal decoding accuracy increased slowly after the addition of the odorant, and increased further after the animal received the reward (Figures 4Ai,iii). When the animal became proficient decoding accuracy increased rapidly beyond 80% after addition of the odorant (Figures 4Aii,iv). For high gamma tPRP the accuracy was higher for the proficient animal for peak-referenced tPRP compared to trough-referenced tPRP (Figure 4Aiv). Figures 4 B and C show mean bar graphs and violin plots for the mean accuracy for decoding contextual odorant identity calculated for the last second of the odorant epoch (1.5 to 2.5 sec after diverting the odorant towards the mouse) for shuffled, naïve, and proficient. Figure 4B shows the accuracy for the peak tPRP and Figure 4C shows the accuracy for trough tPRP. For all conditions the accuracy is significantly higher for the proficient stage compared to naïve or shuffled. GLM analysis finds for both CA1 and mPFC statistically significant differences between naïve vs. proficient and shuffled vs. proficient for both beta and gamma tPRP ($p<0.001$,

297 756 observations, 744 d.f., F-statistic=25.1, $p<0.001$, 6 mice, 8 odor pairs,
298 Supplementary Table 5) and for gamma tPRP GLM finds statistically significant
299 differences between peak and trough ($p<0.001$, 756 observations, 744 d.f., F-
300 statistic=25.2, $p<0.001$, 6 mice, 8 odor pairs, Supplementary Table 5).

301

302 **Coordinated hippocampal-prefrontal neural activity decreased for the unrewarded**
303 **odorant as the animal became proficient.**

304

305 Coordinated hippocampal-prefrontal neural activity supports the organization of brain
306 rhythms and is present during a range of cognitive functions presumably underlying
307 transfer of information between these two brain regions (Colgin, 2011; Gordon, 2011;
308 Headley and Paré, 2017; Lisman et al., 2017). We proceeded to determine whether
309 there were changes in coordinated neural activity between dorsal CA1 and mPFC as
310 the animal learned to discriminate the odorants. We used two complementary methods
311 to quantify coordinated neural activity by calculating coherence and phase locking value
312 (PLV) (Borjigin et al., 2013; Namburi, 2021).

313

314 Figure 5A shows an example of a pseudocolor plot for the time course for coherence for
315 a session where a mouse was engaged in the go-no go task. The pseudocolor plots
316 show the average coherence time course per trial for (i) S+ naïve (ii) S- naïve (iii) S+
317 proficient (iv) S- proficient. For S- the pseudocolor plot shows that a decrease in
318 coherence elicited after the odor onset develops as the mouse becomes proficient
319 (compare Figures 5Aii and iv). Figure 5Bi shows the change of coherence (Δ

coherence) elicited by the odorants as a function of frequency for naïve and proficient mice calculated as the mean per odorant pair per mouse. Δ coherence is defined as the mean coherence in the window from 1.5 to 2.5 sec after the odorant onset minus the mean coherence for -1.5 to 0 sec. We found that the Δ coherence became negative for the unrewarded odorant as the animal became proficient discriminating between odorants. Figures 5Aii to iv show bar graphs/violin plots for per mouse per odorant pair for Δ coherence for the different bandwidths: (ii) theta, (iii) beta, (iv) gamma. A GLM analysis finds for all bandwidths statistically significant differences for Δ coherence for S+ vs. S- and the interaction between S+ vs. S- and naïve vs. proficient ($p<0.001$, 190 observations, 186 d.f., F-statistic=21.6-32.4, $p<0.001$, 6 mice, 8 odor pairs, Supplementary Table 6) and for theta the GLM analysis finds additionally a significant difference between naïve and proficient ($p<0.05$).

Figure 5C shows the odor-elicited change in average PLV (Δ PLV) per mouse per odor pair for (i) theta, (ii) beta, (iii) gamma. Here we also found a negative Δ PLV for the unrewarded odorant for the proficient mice. For Δ PLV GLM finds statistically significant differences for Δ PLV between naïve vs. proficient ($p<0.05$), S+ vs. S- and the interaction between S+ vs. S- and naïve vs. proficient ($p<0.001$, 192 observations, 188 d.f., F-statistic=29.5-46.5, $p<0.001$, 6 mice, 8 odor pairs, Supplementary Table 7). Finally, Figure 5D shows a strong correlation between Δ coherence and Δ PLV for (i) theta, (ii) beta, (iii) gamma. In conclusion, both the Δ coherence and Δ PLV measures indicate that as the mouse becomes proficient there was a decrease in coordinated hippocampal-prefrontal neural activity for the unrewarded odorant.

343

344 **The strength of PAC and peak angle variance differed between the CaMKIIα**
345 **genotypes.**

346

347 Since CaMKIIα is a protein involved in LTP, while PAC plays a role in learning and
348 memory in hippocampal space tasks we asked whether PAC and tPRP differed
349 between the different CaMKIIα genotypes (WT, CaMKIIα Het and CaMKIIα KO). We
350 trained mice from the three genotypes in the go-no go task. There was no difference in
351 the number of sessions to criterion (Figure 6 - Figure supplement 1 A, GLM $p>0.05$, 24
352 observations, 21 d.f., F-statistic=0.26, $p>0.05$, 8 odor pairs, Supplementary Table 8).
353 However, for proficient mice the percent correct was higher for WT compared to both
354 CaMKIIα Het and CaMKIIα KO (Figure 6 - figure supplement 1 B, GLM $p<0.05$, 137
355 observations, 134 d.f., F-statistic=3.7, $p<0.05$, 6 mice, 8 odor pairs, Supplementary
356 Table 8) and the intertrial interval was larger for CaMKIIα Het (Figure 6 - figure
357 supplement 1 B, $p<0.001$, 137 observations, 134 d.f., F-statistic=13.5, $p<0.001$, 6 mice,
358 8 odor pairs, Supplementary Table 8).

359

360 We then asked whether tPAC in the hippocampus and mPFC differs between the
361 different genotypes. When we compared strength of tPAC, measured by the modulation
362 index (MI), and the peak angle variance between genotypes (WT, CaMKIIα Het and
363 CaMKIIα KO), we found significant differences. Figure 6 - figure supplement 2 A, B
364 shows the average MI per mouse per odorant pair for beta (Ai), high gamma (Bi) for
365 hippocampus and for beta (Aii) and gamma (Bii) for prefrontal cortex. For beta tPAC

366 GLM finds a statistically significant difference for MI for the interaction between WT vs.
367 CaMKIIα KO and S+ vs. S- in both the hippocampus and mPFC ($p<0.001$, 544
368 observations, 532 d.f., F-statistic=10.3-34.3, $p<0.001$, 6 mice, 8 odor pairs,
369 Supplementary Table 9). For high gamma tPAC there was an increase in MI for
370 CaMKIIα Het and a decrease in MI for CaMKIIα KO compared to WT and GLM analysis
371 finds a statistically significant difference between WT vs. CaMKIIα KO and WT vs.
372 CaMKIIα Het for both hippocampus and mPFC ($p<0.001$, 544 observations, 532 d.f., F-
373 statistic=10.3-34.3, $p<0.001$, 6 mice, 8 odor pairs, Supplementary Table 9).
374
375 Figure supplement 2C, D shows average peak angle variance per mouse per odorant
376 pair for beta (Ci), high gamma (Ei) in the hippocampus and (Cii) beta, (Eii) high gamma
377 in prefrontal cortex. For proficient mice the peak angle variance for the rewarded
378 odorant decreased for CaMKα Het and increased for CaMKα KO. GLM analysis found a
379 statistically significant difference for WT vs. CaMKIIα Het, WT vs. CaMKIIα KO, naïve
380 vs. proficient and S+ vs. S- for theta/beta and theta/gamma for both the hippocampus
381 and mPFC ($p<0.05$, 544 observations, 532 d.f., F-statistic=20.6, $p<0.001$, 6 mice, 8 odor
382 pairs, Supplementary Table 10).
383
384 **The accuracy for decoding the contextual identity of the odorant decreased in the**
385 **CaMKIIα knockout mouse and was correlated with percent correct discrimination.**
386
387 The differences in PAC between CaMKIIα genotypes raises the question whether
388 decoding of contextual identity from tPRP is altered in the CaMKIIα KO and the

CaMKIIα Het mice. Figure 6 shows the results of our comparison of decoding accuracy between genotypes. Figures 6A and B. show examples for proficient mice of the time course for the accuracy of decoding of odorant contextual identity by LDA trained using tPRP for the EAPA odor pair (Figure 6A theta/beta tPRP, Figure 6B theta/gamma tPRP, i. WT, ii. Het, iii. KO). For the WT and CaMKIIα Het mice the accuracy increases monotonously during the odorant epoch (Figures 6Ai,ii and 6Bi,ii) while for the CaMKIIα KO mouse the accuracy reaches a maximum value after one second and then decreases slightly for the rest of the odorant epoch (Figures 6Aiii and 6Biii). Figures 6C and D show the differences in decoding accuracy between the different genotypes assessed in the window from 1.5 to 2.5 sec after addition of the odorant. For both beta and gamma peak or trough tPAC decoding for both the hippocampus and the mPFC decoding accuracy was lowest for CaMKIIα KO. In addition, for gamma trough tPRP decoding for mPFC the accuracy was highest for WT, and decreased for both CaMKIIα Het and CaMKIIα KO mice (Figure 6Div). For beta tPRP LDA GLM found statistically significant differences for decoding accuracy between WT and KO for all conditions ($p<0.001$) and between WT and Het for peak gamma tPRP in the hippocampus, trough gamma tPRP in mPFC ($p<0.05$, 139 observations, 136 d.f., F-statistic=9.9-34.3, $p<0.001$, 6 mice, 8 odor pairs, Supplementary Table 11).

We then asked whether there was a relationship between contextual odorant identity decoding accuracy and percent correct performance for proficient mice in the go-no go task. Figures 6E and 6F show that there were statistically significant correlations between decoding accuracy and percent correct performance for all the different

conditions. The correlation coefficients were as follows: 0.3 for hippocampal peak beta tPRP, 0.24 for hippocampal peak gamma tPRP, 0.29 for mPFC peak beta tPRP, 0.23 for mPFC peak gamma tPRP, 0.3 for hippocampal trough beta tPRP, 0.36 for hippocampal trough gamma tPRP, 0.29 for mPFC trough beta tPRP and 0.40 for mPFC trough gamma tPRP, and the p value for significance of the correlation coefficient was $p<0.01$. This indicates that the decoding accuracy obtained with tPRP is related to behavioral performance.

Coherent hippocampal-prefrontal neural activity differed between CaMKIIα genotypes

Finally, we asked whether there were differences for coordinated hippocampal-prefrontal neural activity for the different CaMKIIα genotypes. Figure 7A shows that for the proficient mice the absolute value of the change of coherence (Δ coherence) elicited by the odorants tended to be smaller for the CaMKIIα KO. For Δ coherence GLM analysis found statistically significant differences for WT vs. KO (theta $p<0.05$, beta and gamma $p<0.001$, 546 observations, 534 d.f., F-statistic=21.2-33.8, $p<0.001$, 6 mice, 8 odor pairs, Supplementary Table 12). Δ PLV showed the same trends (Figure 7B), but the GLM found no statistically significant differences between WT and KO ($p>0.05$, 512 observations, 500 d.f., F-statistic=25.5-39.9, $p<0.001$, 6 mice, 8 odor pairs, Supplementary Table 13).

Discussion

Santiago Ramon y Cajal described the hippocampus as a quaternary region of the olfactory system with profuse olfactory input through entorhinal cortex (Cajal, 1904), but subsequent studies showed that the hippocampus is involved in neural processing for tasks independent of olfaction such as spatial learning and memory in the Morris water maze (Nakazawa et al., 2004). However, the hippocampus does play a role in olfactory learning. Indeed, recent studies implicate a role for olfactory input through the lateral entorhinal cortex to calbindin-expressing pyramidal cells in the dorsal hippocampal CA1 for neural processing of decision-making in the go-no go olfactory discrimination task and these investigators show that these pyramidal cells develop more selective spiking responses to odorants as the animal becomes proficient (Li et al., 2017). Furthermore, studies of oscillatory neural activity implicate directional coupling from the olfactory bulb to the hippocampus in go-no go olfactory discrimination learning (Gourevitch et al., 2010; Martin et al., 2007). In addition, Granger directionality analysis finds that distinct low frequency oscillation bandwidths link the olfactory bulb and hippocampus in a bi-directional manner (Nguyen Chi et al., 2016). Interestingly, mPFC has also been proposed as a downstream information processing brain area coupled with the olfactory bulb. Coupling of low frequency oscillations between the olfactory bulb and mPFC increases during freezing periods in auditory conditioned fear learning (Moberly et al., 2018) and at rest there is strong coupling of low frequency oscillations for both olfactory bulb-hippocampus and olfactory bulb-mPFC (Mofleh and Kocsis, 2021). Furthermore, a recent study found that beta and theta synchrony between mPFC and olfactory regions

457 was elevated as rats switched their attention to odors (Cansler et al., 2021). These
458 findings indicate that the hippocampus and mPFC are coupled to the olfactory bulb
459 through neural oscillatory activity and that these circuits play a role in learning and
460 attention. Taken together with the fact that in a previous publication we showed that
461 when mice become proficient in discriminating odorants in the go-no go task contextual
462 odorant identity can be decoded from beta and gamma tPRP (Losacco et al., 2020)
463 these findings raise the question whether coupled oscillations in mPFC and the
464 hippocampus play a role in olfactory discrimination in go-no go associative learning.

465

466 In this study we found that for both the dorsal CA1 and mPFC as animals became
467 proficient in the go-no go task there was an increase in the variance of the peak angle
468 for beta and high gamma tPAC for the unrewarded odorant (Figure 2) accompanied by
469 a decrease in tPRP for this odorant (Figure 3). This decrease in tPRP for S- was
470 accompanied by a small increase in tPRP for the rewarded odorant resulting in a sharp
471 increase in accuracy for decoding of the contextual odorant identity as the animal
472 became proficient differentiating between odorants (Figure 4). Likewise, decreases in
473 coordinated prefrontal-hippocampal activity elicited by the unrewarded odorant became
474 larger suggesting uncoupling of oscillations in these two brain areas for the unrewarded
475 odorant. When we tested CaMKIIα KO mice, known to be deficient in spatial learning
476 and memory, we found a decrease in the accuracy of the decoding of contextual
477 odorant identity (Figure 6), and a decrease in the magnitude of the decrease in odorant-
478 elicited changes in coherence (Figure 8). Finally, the behavioral performance for
479 CaMKIIα KO and CaMKIIα Het mice was lower than the performance of WT mice

480 (Figure 6 – figure supplement 1) and the accuracy for decoding of contextual odorant
481 identity from tPAC correlated with behavioral performance (Figure 6). These findings
482 indicate that coordinated oscillatory neuronal activity in the hippocampal-mPFC axis
483 plays a role in learning in the go-no go task for olfactory discrimination.

484

485 Theta frequency stimulation, eliciting intrinsic gamma frequency oscillations, is known to
486 be essential for long-term potentiation a process that is thought to be crucial for learning
487 (Bliss and Lomo, 1973; Butler et al., 2016; Larson and Munkácsy, 2015) and theta PAC
488 of higher frequency bursts is thought to be important for information transfer within and
489 between brain regions which is thought to be essential for learning (Fries, 2005). In the
490 hippocampus high frequency oscillations at different phases of theta carry different
491 information. Indeed, Siegle and Wilson used closed loop optogenetics to stimulate
492 parvalbumin (PV) interneurons showing that when PV interneurons are stimulated at the
493 peak of theta mice increased performance in the encoding epoch for a spatial
494 navigation task whereas when they stimulated at the trough of theta mice increased
495 performance in the retrieval epoch (Siegle and Wilson, 2014). Interestingly, here we find
496 that as the animal becomes proficient the variance of the peak angle of PAC increases
497 substantially for the unrewarded odorant (Figure 2). As a result, if the gamma or beta
498 frequencies were being read by a downstream observer at a fixed angle, the information
499 conveyed by oscillations elicited by the rewarded odorant would be missed because of
500 the constantly changing theta phase angle. In contrast, the peak angle variance for the
501 rewarded odorant is small, and presumably this would result in more faithful reading of
502 this information. This is likely what underlies the increased accuracy for decoding the

503 contextual odorant identity from beta and gamma tPRP we found in the proficient
504 mouse (Figure 4). Thus, we found that in the go-no go task phase-referenced power
505 carries information on contextual odorant identity.

506

507 Full genetic knockout of CaMKIIα results in impairments in hippocampus-dependent
508 cognitive tasks and impaired LTP and LTD in adult mice (Coultrap et al., 2014; Silva et
509 al., 1992b). In contrast, although CaMKIIα Het mice share some behavioral deficits with
510 the full CaMKIIα KO including deficient learning and memory in the Morris water maze
511 and deficient retention of contextual fear conditioning (Frankland et al., 2001; Silva et
512 al., 1996), adult CaMKIIα Het mice have additional working memory deficits such as
513 repeat entry errors in the radial arms version of the Morris water maze (Matsuo et al.,
514 2009; Yamasaki et al., 2008). In addition, while young (p 12-16) CaMKIIα Het show LTP
515 of the same magnitude as WT mice in CA1, young adult (9-11 week old) mice display
516 impaired basal synaptic transmission, but do not have a deficit in LTP (Goodell et al.,
517 2016) suggesting the development of compensatory mechanisms for LTP in the Het.
518 PAC plays a role in hippocampal learning and memory (Siegle and Wilson, 2014)
519 raising the question whether the CaMKIIα Het and CaMKIIα KO have deficits in cross
520 frequency coupling. Here we performed to our knowledge the first study to determine
521 whether CaMKIIα-deficient mice display altered PAC. We find that the accuracy for
522 decoding of contextual odorant identity from beta and gamma tPRP is decreased in
523 CaMKIIα KO mice, but not in CaMKIIα Hets (with the exception of a decrease accuracy
524 for mPFC gamma trough tPRP decoding, Figure 6). Interestingly, the strength of PAC,
525 measured as the MI, was highest for gamma tPAC CaMKIIα Hets compared to both WT

526 and CaMKIIα KO (Figure 6 -Figure Supplement 1B). For CaMKIIα Hets the peak angle
527 variance decreased significantly for the rewarded odorant when the animal became
528 proficient (Figure 6 -Figure Supplement 1C,D). If a downstream neural observer is
529 evaluating contextual odorant identity by observing beta or gamma frequency bursts in
530 phase with theta oscillations these changes in PAC for CaMKIIα Hets would tend to
531 increase the ability to discriminate. Thus, the differences found for tPAC for CaMKIIα
532 Hets may be compensatory leading to no difference in decoding accuracy between WT
533 and CaMKIIα Hets (Figure 6). This would agree with the interpretation by Goodell et al.
534 who indicated that LTP deficits in CaMKIIα Hets are restored by compensatory changes
535 during development (Goodell et al., 2016). Finally, given that CaMKIIα Hets have a
536 phenotype reminiscent of schizophrenia it is interesting that resting-state gamma tPAC
537 has been found to be increased in patients with schizophrenia compared to that in
538 healthy controls (Won et al., 2018). These authors speculate that increased tPAC may
539 be related to the compensatory hyper-arousal patterns of the dysfunctional default-
540 mode network in schizophrenia.

541

542 Whether the PAC/tPRP changes found in CaMKIIα Het and CaMKIIα KO mice are due
543 to the decreased expression of CaMKIIα protein or to developmental changes in circuits
544 known to change in these mice such as in the dentate gyrus is an open question that
545 will require future studies with temporally and spatially restricted changes in CaMKIIα
546 activity. CaMKIIα may alter plasticity of pyramidal neurons in CA1 or mPFC.
547 Furthermore, a decrease in CaMKIIα expression may alter the the postsynaptic
548 regulation by CaMKIIα of inhibitory synapse transmission onto the pyramidal neurons

549 (Cook et al., 2021; Udakis et al., 2020). Finally, a subpopulation of granule cells that
550 play a role in odorant discrimination in the go/no go task are found in the olfactory bulb
551 and these cells are involved in generating the gamma frequency oscillatory activity in
552 the bulb (Malvaut et al., 2017). The olfactory bulb granule cells may be involved in
553 changing coordinated oscillations between the olfactory bulb and hippocampus in the
554 CaMKIIα KO/Het mice.

555

556 In conclusion we found that as the mouse learns to differentiate odorants in the go-no
557 go associative learning task there are changes in PAC that result in an increase of the
558 accuracy of decoding of the contextual odorant identity from tPRP. We found that as the
559 animal becomes proficient the coordinated neural activity between CA1 and mPFC
560 decreases for the unrewarded odorant. Finally, the accuracy of decoding the contextual
561 odorant identity from tPRP decreased in the CaMKIIα KO, but did not decrease in the
562 CaMKIIα Het and this decoding accuracy correlated with behavioral performance across
563 genotypes.

564

565

Materials and methods

Key Resources Table

REAGENT TYPE	REAGENT or RESOURCE	SOURCE	IDENTIFIER	ADDITIONAL INFORMATION
Chemical compound, drug	Isoamyl acetate	Sigma-Aldrich	Cat#123-92-2	Odorant
Chemical compound, drug	Ethyl acetate	Sigma-Aldrich	Cat# 141-78-6	Odorant
Chemical compound, drug	Propyl acetate	Sigma-Aldrich	Cat# 109-60-4	Odorant
Chemical compound, drug	Mineral oil	Sigma-Aldrich	Cat# 8042-47-5	Odorant
Chemical compound, drug	Acetophenone	Sigma-Aldrich	Cat# 98-86-2	Odorant
Chemical compound, drug	Ethyl benzoate	Sigma-Aldrich	Cat# 93-89-0	Odorant
Other	Nickel-chrome wire	Sandvik	Cat#PX000002	Tetrode fabrication
Other	16 Channel Electrode Interface Board	Neuralynx	EIB-16	Tetrode fabrication
Software, algorithm	Analysis code	This paper	Available on github and by request	https://github.com/restrepd/drgMaster
Strain, strain background	Mouse: CaMKIIα WT	Bayer Lab	Coultrap et al., 2014	Male mice
Strain, strain background	Mouse: CaMKIIα HET	Bayer Lab	Coultrap et al., 2014	Male mice
Strain, strain background	Mouse: CaMKIIα KO	Bayer Lab	Coultrap et al., 2014	Male mice
Software, algorithm	MATLAB_R2018a	Mathworks	RRID: SCR_001622	
Software, algorithm	Illustrator	Adobe	RRID: SCR_010279	
Software, algorithm	Photoshop	Adobe	RRID: SCR_014199	

571 **Animals**

572 Littermate mice with genotypes of CaMKIIα KO, Het and WT were obtained from
573 heterozygous breeding (Coultrap et al., 2014). Mice were housed in a vivarium with a
574 reversed light cycle of 14/10 h light/dark periods with lights on at 10:00 p.m. Food
575 (Teklad Global Rodent Diet no. 2918; Harlan) was available ad libitum. Access to water
576 was restricted during the behavioral sessions. However, if mice did not obtain ~1ml of
577 water during the behavioral session, additional water was provided in a dish in the cage
578 (Slotnick and Restrepo, 2005). All mice were weighed daily and received sufficient
579 water to maintain >80% of the weight before water restriction. All experiments were
580 performed according to protocols approved by the University of Colorado Anschutz
581 Medical Campus Institutional Animal Care and Use Committee.

582

583 **Surgery and double tetrode implantation**

584 Male mice 2-4 months of age were anesthetized by brief exposure to isoflurane (2.5%)
585 and subsequently anesthesia was maintained with an intraperitoneal injection of
586 ketamine (100 mg/kg) and xylazine (10 mg/kg). The tetrode drive included one optical
587 fiber ferrule for support of an EIB 8 board with 2 tetrodes with four polyamide-coated
588 nichrome wires (diameter 12.5 μm; Sandvik, gold plated to an impedance of 0.2–
589 0.4MΩ). Tetrodes were connected, and the optic fiber ferrule was glued through an EIB-
590 8 interface board (Neuralynx). Mice were implanted with two tetrode drives aimed at
591 mPFC (+1.94 mm anterior, +0.25 mm lateral, and -3.12 mm below bregma) (Eleore et
592 al., 2011) and the second tetrode drive at the right CA1 layer of the dorsal hippocampus
593 (-3.16 mm posterior, +3.2 mm lateral, and -2 mm below bregma) (Eleore et al.,

594 2011)(Fig. 1A). One ground screw was inserted 1 mm posterior from bregma and 1 mm
595 lateral to the midline and sealed to the bone with dental acrylic. Mice were allowed to
596 recover for 1 week before the initiation of the behavioral studies. All behavioral and LFP
597 recording experiments were performed with 2.5-8 month old mice that had undergone
598 double tetrode drive implantation.
599

600 **Go-No-Go Behavioral Task**

601 We used the methods previously described in (Losacco et al., 2020). Briefly, water-
602 restricted mice were required to enter an odor port and lick at the water spout to initiate
603 the release of the odorants 1–1.5 s after the first lick (Figs. 1B,C). Mice were required to
604 lick at least once in four 0.5 s intervals during reinforced odorant delivery (S+) to obtain
605 10 µl of water. When exposed to the unreinforced odorant (S–), mice refrain from licking
606 for 2 sec because of the effort it takes to lick for this period. Licking was detected by
607 closing a circuit between the licking spout and the grounded floor of the cage (Slotnick
608 and Restrepo, 2005). The performance of the mice was assessed by calculating correct
609 response to the S+ and S– odorants in 20 trial blocks where 10 S+ and 10 S– odorants
610 were presented at random. Mice were first trained to discriminate between 1% isoamyl
611 acetate (S+) and mineral oil (S-). Once the mice learned to discriminate between
612 isoamyl acetate and mineral oil (percent correct > 80% in two blocks) the odorant pair
613 was switched to the 1% Acetophenone S+ and Ethyl Benzoate S- (APEB) odorant pair.
614 Once the mice learned to discriminate between acetophenone and ethyl benzoate
615 acetate the odor pair was reversed. Ethyl Benzoate became the S+ and Acetophenone
616 the S- (EBAP). When the mice became proficient at the reversal, the odor pair was

switched. The same pattern was followed for the rest of the odor pairs (see Table1 for the list of all odorants used). All odorants were obtained from Sigma-Aldrich and were diluted in mineral oil at room temperature. Mice were trained until they performed at 80 percent correct or better in the last two blocks of 20 trials. Fig. 2B shows an example of the percent correct odorant discrimination performance per trial. We did not find significant differences in the analysis between odorant pairs.

Double tetrode recordings

We followed procedures as previously described (Li et al., 2015). The mouse was recorded within the olfactometer chamber with dimensions of 11.6 × 9.7 × 9.4 cm. The EIB-8 boards that recorded signals from the tetrodes were connected to an INTAN RHD2132 16 channel amplifier/A/D converter that interfaced with an RHD2000 USB interface board. Extracellular potentials from the tetrodes were captured, filtered with either a 500 Hz or a 5 kHz low pass filter, and digitized at 20 kHz. Meta data for the behavioral events such as valve opening/closing times and odor identity were recorded through a digital output from the olfactometer. Licks detected by the olfactometer were recorded as an analog signal by the INTAN board.

PAC Analysis

As previously described in Losacco et al. (2020), phase amplitude coupling (PAC) data were processed using the Hilbert transform using a method described by Tort et al. (2010). Briefly, the signal was bandpass filtered with a 20th order Butterworth filter using Matlab's filtfilt function with zero phase shift to extract LFP in the low frequency

oscillation used for phase estimation and the high frequency oscillation used for estimation of the amplitude of the envelope (Figure 1Ei,ii). The Hilbert transform established the theta (6-14 Hz) phase and the envelope for beta (15-30 Hz) and high gamma (65-95 Hz, referred to as gamma) (Figures 1Eiii,iv). To quantify the strength of PAC, we calculated the modulation index (MI). If PAC is non-existent, MI = 0, meaning the mean amplitude is distributed uniformly over theta phases, and if PAC is a delta function MI = 1. MI for signals measured in brain areas such as the hippocampus typically fall between 0–0.03 (Tort et al., 2010).

PRP Analysis

As previously described in Losacco et al. (2020), we developed the PRP approach using custom MATLAB code. PAC was calculated following the approach used by Tort et al. (2010), as described in PAC analysis and summarized in Figure 1. Peak and trough theta phases are defined as the phase for maxima and minima of the PAC distribution measured for the S+ trial. A continuous Morlet wavelet transform was used to estimate the power for the high frequency oscillations (Buonviso et al., 2003). PRP was estimated as the power of the high frequency oscillations measured at the peak or trough of PAC. The MATLAB code used for data analysis has been deposited to https://github.com/ restrepd/drgMaster.

Coherence and Phase Locking Value (PLV) Analysis

In order to quantify the interaction of LFP oscillations from electrodes impaled into different brain regions we computed the complementary values of coherence and phase

663 locking value (PLV). We measured coherence following the method detailed in the
664 supplemental information of (Borjigin et al., 2013). Briefly, coherence between LFP
665 channels is measured by amplitude squared coherence $C_{xy}(f)$ where f is frequency
666 (mscohere.m in the MATLAB signal toolbox; MathWorks, Inc.). This is a coherence
667 estimate of the input signals x and y using Welch's averaged, modified periodogram
668 method. The magnitude squared coherence estimate $C_{xy}(f)$ is a function of frequency
669 with values between 0 and 1 that indicates how well x corresponds to y at each
670 frequency. Furthermore, we quantified phase-locking between the two LFPs by
671 computing PLV following the procedure detailed by Lachaux et al. (1999) using
672 MATLAB code generated by Praneeth Namburi (Namburi, 2021). Briefly, we compute
673 the convolution of each LFP with a complex Gabor wavelet centered at frequency f and
674 then we compute the PLV as the normalized absolute value of the sum of the
675 exponential of the difference in phase multiplied by the imaginary number i. If the phase
676 difference between the two LFPs varies little across the trials, PLV is close to 1; it is
677 close to zero when the relationship between the phases varies randomly across trials.
678

679 **Statistical analysis**

680 The statistical analysis was done as described in Losacco et al. (2020) using MATLAB
681 code. Both PAC and PRP parameters were calculated separately per electrode (16
682 electrodes per mouse, 8 hippocampus, 8 mPFC) for all electrodes per mouse. Statistical
683 significance for changes in measured parameters for multivariate factors such as the
684 mouse genotype, naïve vs. proficient and S+ vs. S-, and the interactions of these factors
685 was estimated using generalized linear model (GLM) analysis, with post-hoc tests for all

686 data pairs corrected for multiple comparisons using false discovery rate (Curran-Everett,
687 2000). The post hoc comparisons between sets of data were performed either with a t-
688 test, or a ranksum test, depending on the result of an Anderson-Darling test of
689 normality. Degrees of freedom and statistical significance have the same meaning in
690 GLM as in analysis of variance and regression (Agresti, 2015). In addition, as a
691 complementary assessment of significant differences (Halsey et al., 2015) we display
692 95% confidence intervals (CIs) shown in the figures as vertical black lines or shadow
693 boundaries that was estimated by bootstrap analysis of the mean by sampling with
694 replacement 1000 times.
695

696 **Linear discriminant analysis**

697 Decoding of contextual odorant identity from tPRP values was performed using linear
698 discriminant analysis (LDA) using MATLAB code as described in Losacco et al. (2020).
699 LDA was trained by a leave one out procedure where the algorithm was trained with all
700 trials but one, and the accuracy was assessed by predicting the odorant identity for the
701 trial that was left out. This was repeated for all trials and was performed separately for
702 peak and trough PRP, and for analysis where the identity of the odorants was shuffled.
703 LDA was performed on a per-mouse basis where the input was the PRP recorded from
704 16 electrodes.
705

706 **Acknowledgements**

707 We thank Ms. Nicole Arevalo for animal husbandry and Ms. Dnate' Baxter for laboratory
708 support. We thank Dr. Stephen Coultrap for helpful discussion and animal support and
709 Mrs. Lauraine Mediavillo for assistance in collecting data. This research was supported
710 by an Administrative Supplement S1 to NIH UF1 NS116241 (to DRG), NIH R01
711 NS081248 (to KUB), NIH R01 DC000566 (to DR) and by a pilot grant from the Center
712 for NeuroScience (CNS) of the University of Colorado School of Medicine (to KUB and
713 DR).

714

715 **Competing interests.** DR declares no competing interests.

716

717 **Table 1. Odorant pairs**

Name	Rewarded odorant (S+)	unrewarded odorant (S-)
APEB	1% Acetophenone	1% Ethyl benzoate
EBAP	1% Ethyl benzoate	1% Acetophenone
EAPA1	0.1% Ethyl acetate	0.05% Ethyl acetate + 0.05% Propyl acetate
EAPA1	0.05% Ethyl acetate + 0.05% Propyl acetate	0.1% Ethyl acetate
EAPA2	0.01% Ethyl acetate	0.005% Ethyl acetate + 0.005%Propyl acetate
PAEA2	0.005% Ethyl acetate + 0.005% Propyl acetate	0.01% Ethyl acetate
EAPA3	0.001% Ethyl acetate	0.0005% Ethyl acetate + 0.0005% Propyl acetate
PAEA3	0.0005% Ethyl acetate + 0.0005%Propyl acetate	0.001% Ethyl acetate

718

719 The odorants were diluted in odorless mineral oil.

720

721 **Table 2. Number of sessions and number of mice per odorant pair**

Odorant pair	# of mice	Total sessions
1% Acetophenone vs 1% Ethyl benzoate	6 WT 7 Het 5 KO	22 22 11
1% Ethyl benzoate vs 1% Acetophenone	6 WT 7 Het 5 KO	22 55 29
0.1% Ethyl acetate vs 0.05% ethyl acetate + 0.05% propyl acetate	6 WT 7 Het 5 KO	15 23 17
0.05% ethyl acetate + 0.05% propyl acetate vs 0.1% Ethyl acetate	6 WT 7 Het 5 KO	17 35 37
0.01% Ethyl acetate vs 0.005% ethyl acetate + 0.005% propyl acetate	6 WT 7 Het 4 KO	23 52 24
0.005% ethyl acetate + 0.005% propyl acetate vs 0.01% Ethyl acetate	6 WT 7 Het 4 KO	31 49 21
0.001% Ethyl acetate vs 0.0005% ethyl acetate + 0.0005% propyl acetate	6 WT 7 Het 3 KO	60 64 16
0.0005% ethyl acetate + 0.0005% propyl acetate vs 0.001% Ethyl acetate	6 WT 7 Het 3 KO	34 57 13

722

723

724

725

726

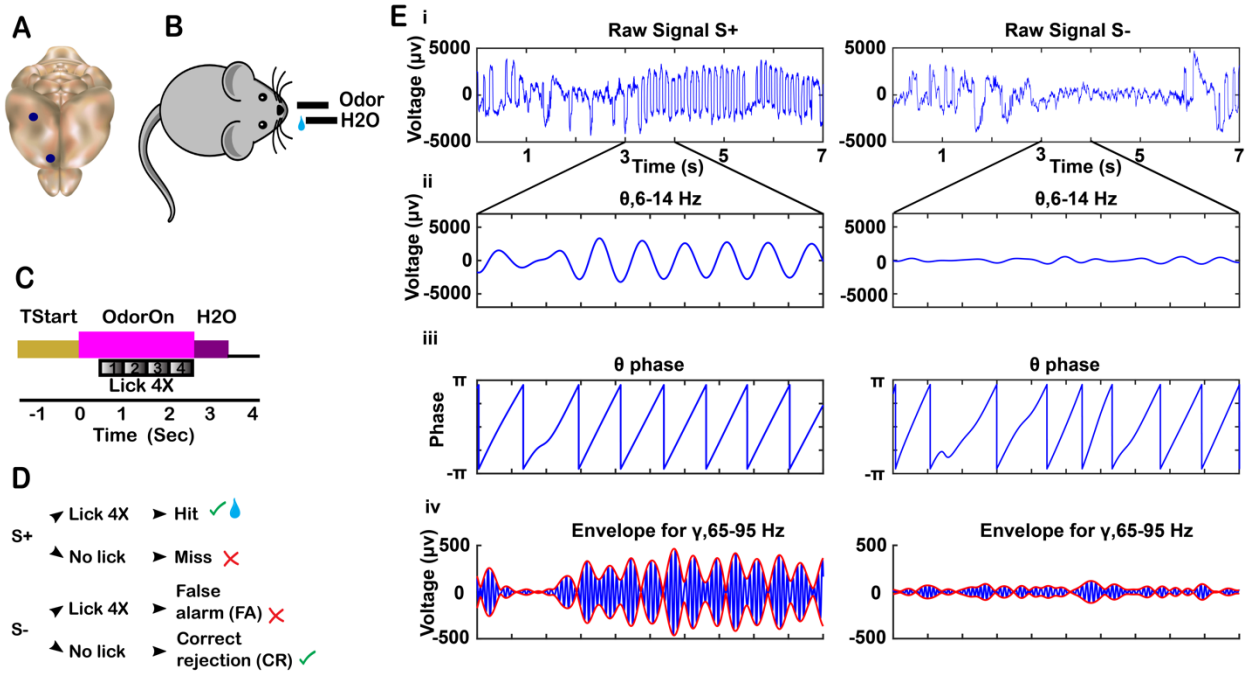

Figure 1. Tetrode location, behavioral task and PAC analysis.

(A) Mouse brain showing location of tetrodes in CA1 and mPFC. (B) Mouse undergoing odor discrimination behavioral task. Mouse self-initiates trials by licking the lixit closing the lick detection circuit. Odorants and water were delivered according to the timeline in C and the decision tree in D. (C) Timeline for a single trial. When the animal entered the port and licked at the lixit, it started the trial. TStart (1-1.5 sec) is the time from initiation of the trial to odor delivery. At time 0 the final valve air flow was turned towards the odor port for 2.5 sec resulting in odor onset ~100 ms after the valve was activated (Losacco et al., 2020). To obtain the water reward for the rewarded odorant (S+) the mouse must lick at least once during each 0.5 s block for four blocks in the response area. If the stimulus is the rewarded odorant and the animal licked, a water reward was delivered (Hit). If the animal did not lick in each 0.5 sec block (Miss), water was not delivered. When the odorant was the unrewarded odorant (S-) the mouse was not rewarded with water regardless of whether it licked in all 0.5 sec blocks (False Alarm, FA) or not

742 (Correct Rejection, CR). (D) Decision tree for each trial. Green check mark indicates the
743 correct decision was made. Red “X” mark indicates an incorrect decision was made.
744 Water reward is represented by the water droplet symbol. (E) PAC data analysis for the
745 LFP. For each electrode, the raw signal collected at 20 kHz (i. rewarded odorant [left],
746 unrewarded odorant right) was filtered into different frequency bands (ii. theta 6-14 Hz).
747 Hilbert transform was used to calculate the theta phase (iii) and the amplitude envelope
748 of higher oscillations such as high gamma (65-95 Hz) (red line in v; blue line is the
749 gamma filtered LFP).
750
751

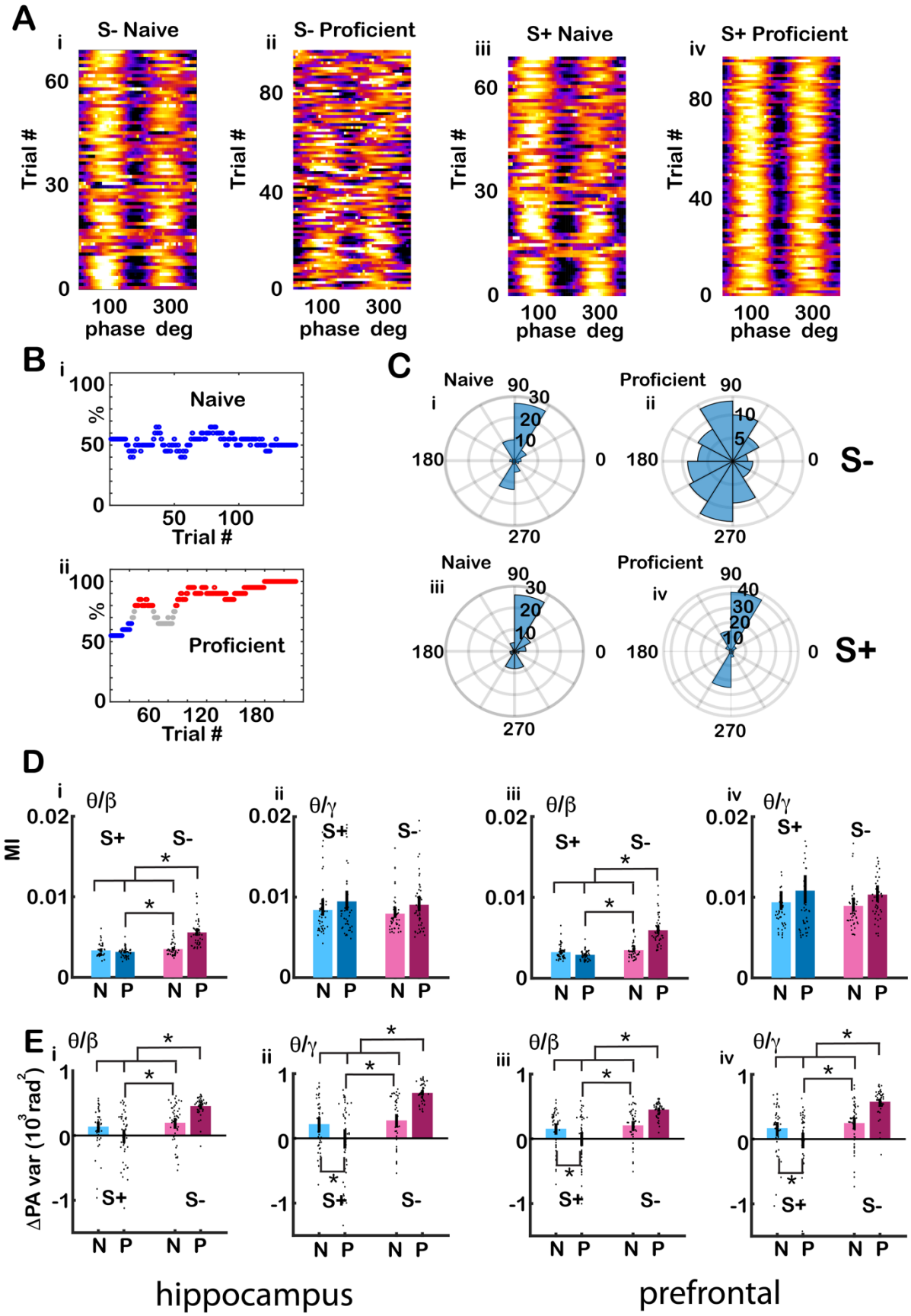
A
i S- Naive
ii S- Proficient
iii S+ Naive
iv S+ Proficient
Trial #
phase deg
B
Naive
Proficient
%
Trial #
C
Naive
Proficient
S-
S+
D
θ/β
θ/γ
MI
S+
S-
N P
E
ΔPA var (10^3 rad^2)
hippocampus
prefrontal

752

Figure 2. The peak angle variance of PAC increased for the unrewarded odorant as the animal learned to discriminate odorants.

(A) Pseudocolor plots showing the phase amplitude relationship for the unrewarded odorant S- (left) and rewarded odorant S+ (right) for two example sessions (naïve and proficient) of the go-no-go task. As the animal became proficient differentiating between the rewarded and unrewarded odorants, PAC peak angle appeared to become more variable for the unrewarded odorant (S-) compared to the rewarded odorant (S+). (B) Behavioral performance for the two sessions. (i) During the naïve stage, the animal licked for the presentation of the rewarded and unrewarded odorants (performance ~50%). (ii) During the proficient stage (red points), the animal licked more frequently during the presentation of the rewarded odorant and refrained from licking during the presentation of the unrewarded odorant. Blue = percent correct < 65%, red percent correct >80%. (C) Peak angle polar histograms for (i) naïve S- (ii) proficient S- (iii) naïve S+ and (iv) proficient S+. The variance of the peak angle appears to increase for the S- in comparison to the S+ during the proficient stage. (D) Bar graphs and violin plots showing the differences in MI between S+ and S- for hippocampus (i)theta/beta (ii) theta/high gamma and mPFC (iii) theta/beta (iv) theta/high gamma. For the beta tPAC for both the hippocampus and mPFC GLM finds statistically significant differences for S+ vs. S- and for the interaction between S+ vs. S- and naïve vs. proficient ($p<0.001$, 188 observations, 184 d.f., F-statistic=51,67.7, $p<0.001$, 6 mice, 8 odor pairs, Supplementary Table 1). (E) Bar graphs showing differences for peak angle variance between S+ and S- for hippocampus (i) for theta/beta (ii) theta/high gamma and mPFC (iii) theta/beta (iv) theta/high gamma. For both beta and gamma tPAC and for both the

776 hippocampus and mPFC GLM finds statistically significant differences for S+ vs. S- and
777 for the interaction between S+ vs. S- and naïve vs. proficient ($p<0.001$, 188
778 observations, 184 d.f., F-statistic=19.5-26.4, $p<0.001$, 6 mice, 8 odor pairs,
779 Supplementary Table 2). Asterisks show significant p values ($p<pFDR$) for post-hoc
780 pairwise tests.
781
782

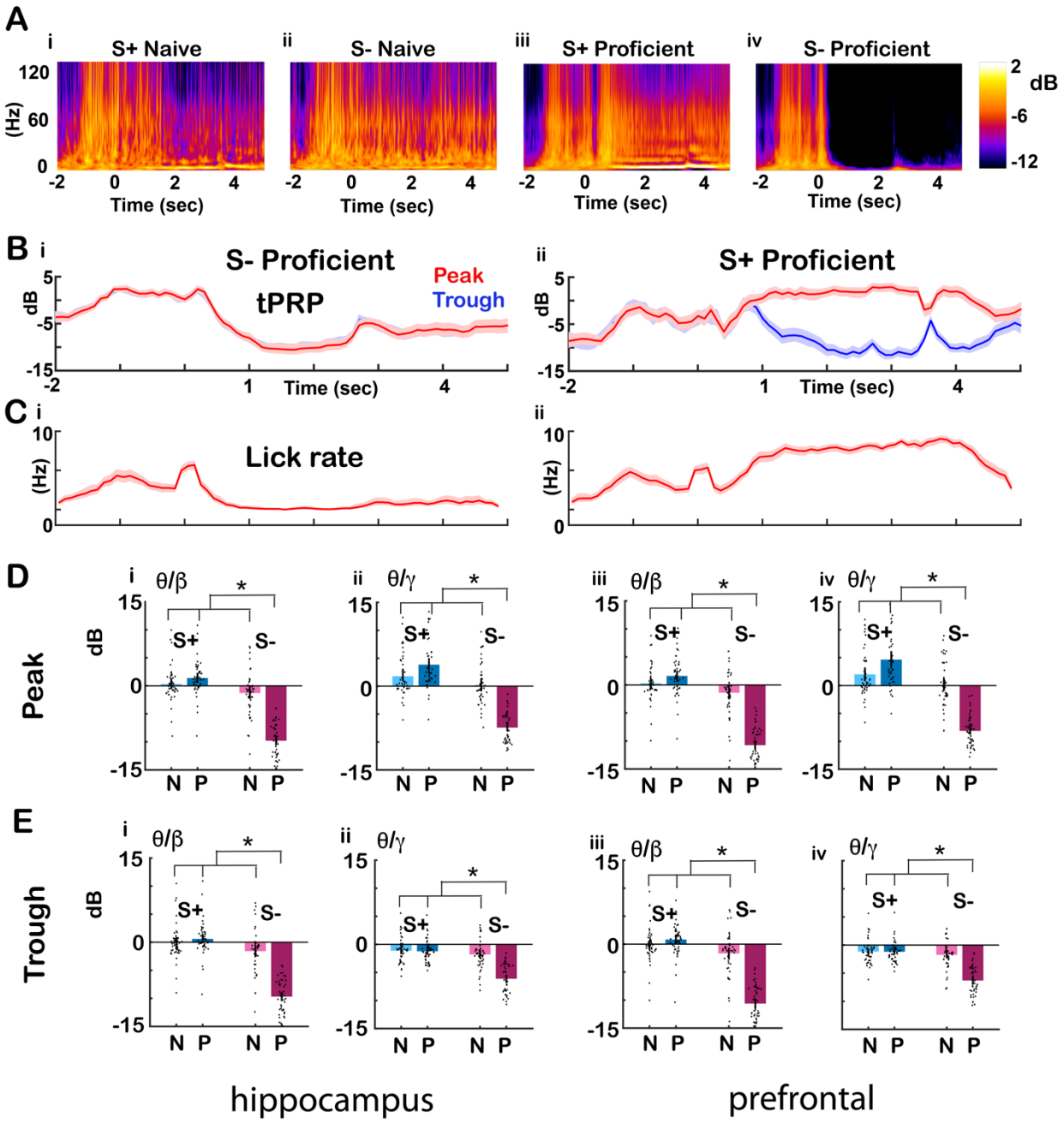

Figure 3. Changes in phase referenced power as the animal became proficient

(A) Examples of the time course per trial for the average wavelet broadband LFP spectrogram for (i) S+ naïve (30 trials) (ii) S- naïve (27 trials) (iii) S+ proficient (84 trials) (iv) S- proficient (84 trials). Pseudocolor scale for LFP power is shown in dB. (B) Average gamma wavelet power referenced to theta peak and through for the same trials

789 as shown in A (i) S- proficient (ii) S+ proficient, red: peak, blue: through, shadow:
790 confidence interval. (C) Lick rate for the same trials (i) S- proficient (ii) S+ proficient.
791 (D,E) Summary bar graphs/violin plots showing that peak tPRP decreases for S- as the
792 mice become proficient. D: peak, E: through, (i) theta/beta and (ii) theta/gamma
793 hippocampus (iii) theta/beta and (iv) theta/gamma prefrontal cortex. GLM finds
794 statistically significant differences for S+ vs. S- and for the interaction between S+ vs. S-
795 and naïve vs. proficient ($p<0.001$, 376 observations, 368 d.f., F-statistic=72.7-103,
796 $p<0.001$, 6 mice, 8 odor pairs, Supplementary Table 3). Asterisks show significant p
797 values ($p<pFDR$) for post-hoc pairwise tests.
798

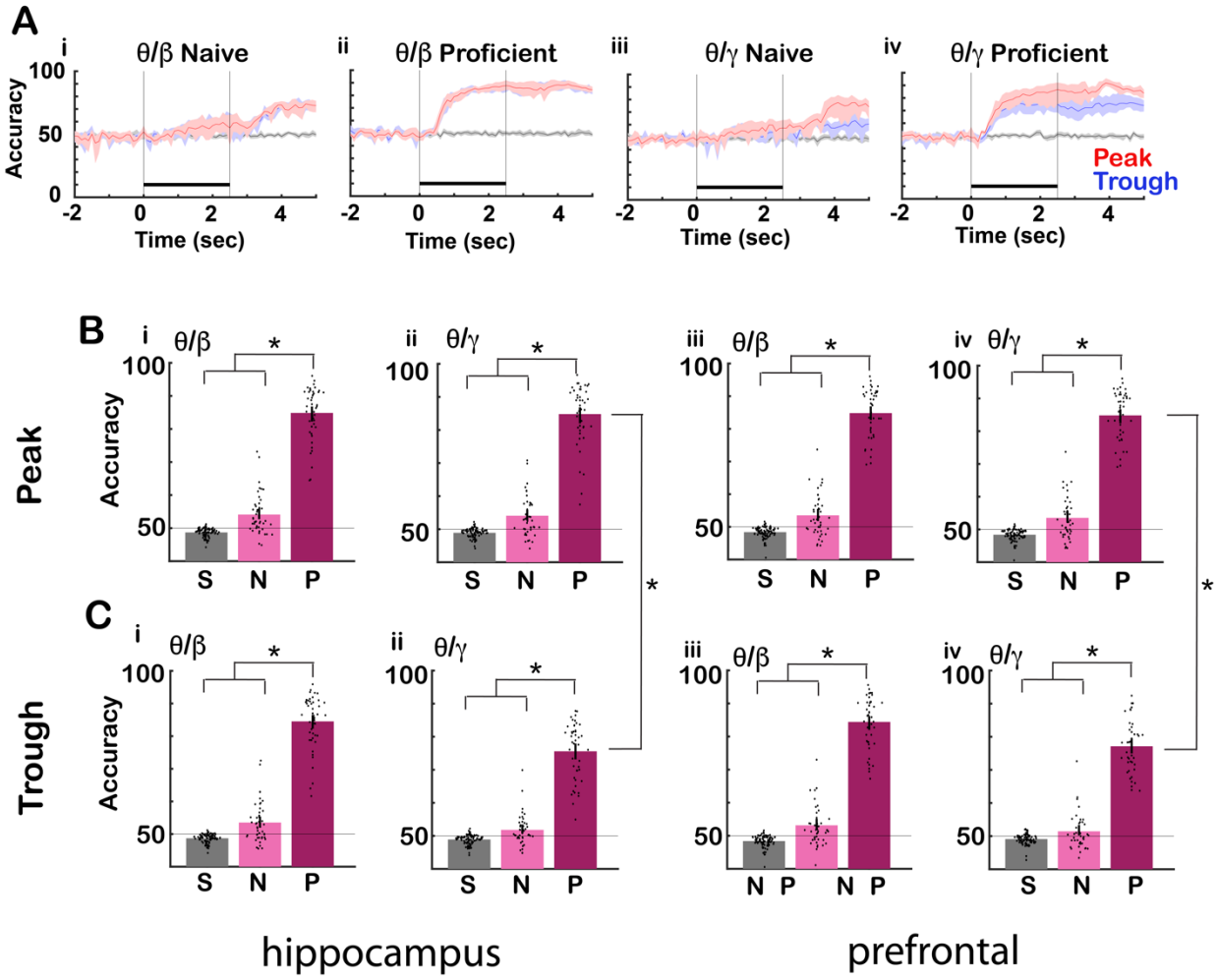

Figure 4. Linear discriminant analysis for decoding the contextual odorant identity from tPRP

A. Example for one mouse for the time course for the accuracy of odorant identity decoding by a linear discriminant analysis algorithm trained using tPRP for the EAPA odor pair (i) naïve theta/beta, (ii) proficient theta/beta, (iii) naïve theta/gamma, (iv) proficient theta/gamma red: peak, blue: through, black: shuffled, shadow: confidence interval, black bar: odorant application. B and C. Bar graphs/violin plots showing the differences in decoding accuracy between shuffled, naïve, and proficient. B: Accuracy for peak tPRP for (i) theta/beta in the hippocampus, (ii) theta/gamma in the

809 hippocampus, (iii) theta/beta in mPFC, (iv) theta/gamma in mPFC. C: Accuracy for
810 through for (i) theta/beta in the hippocampus, (ii) theta/gamma in the hippocampus, (iii)
811 theta/beta in mPFC, (iv) theta/gamma mPFC. The bars show the average accuracy, and
812 the points are the accuracy per mouse per odor pair. The vertical bars show the
813 confidence interval. For beta and gamma tPRP LDA GLM finds statistically significant
814 differences for naïve vs. proficient and shuffled vs. proficient ($p<0.001$, 756
815 observations, 744 d.f., F-statistic=25.1, $p<0.001$, 6 mice, 8 odor pairs, Supplementary
816 Table 5). For gamma tPRP LDA GLM finds statistically significant differences between
817 peak and trough ($p<0.001$, 756 observations, 744 d.f., F-statistic=25.2, $p<0.001$, 6 mice,
818 8 odor pairs, Table S4). Asterisks show significant p values ($p<pFDR$) for post-hoc
819 pairwise tests.
820
821

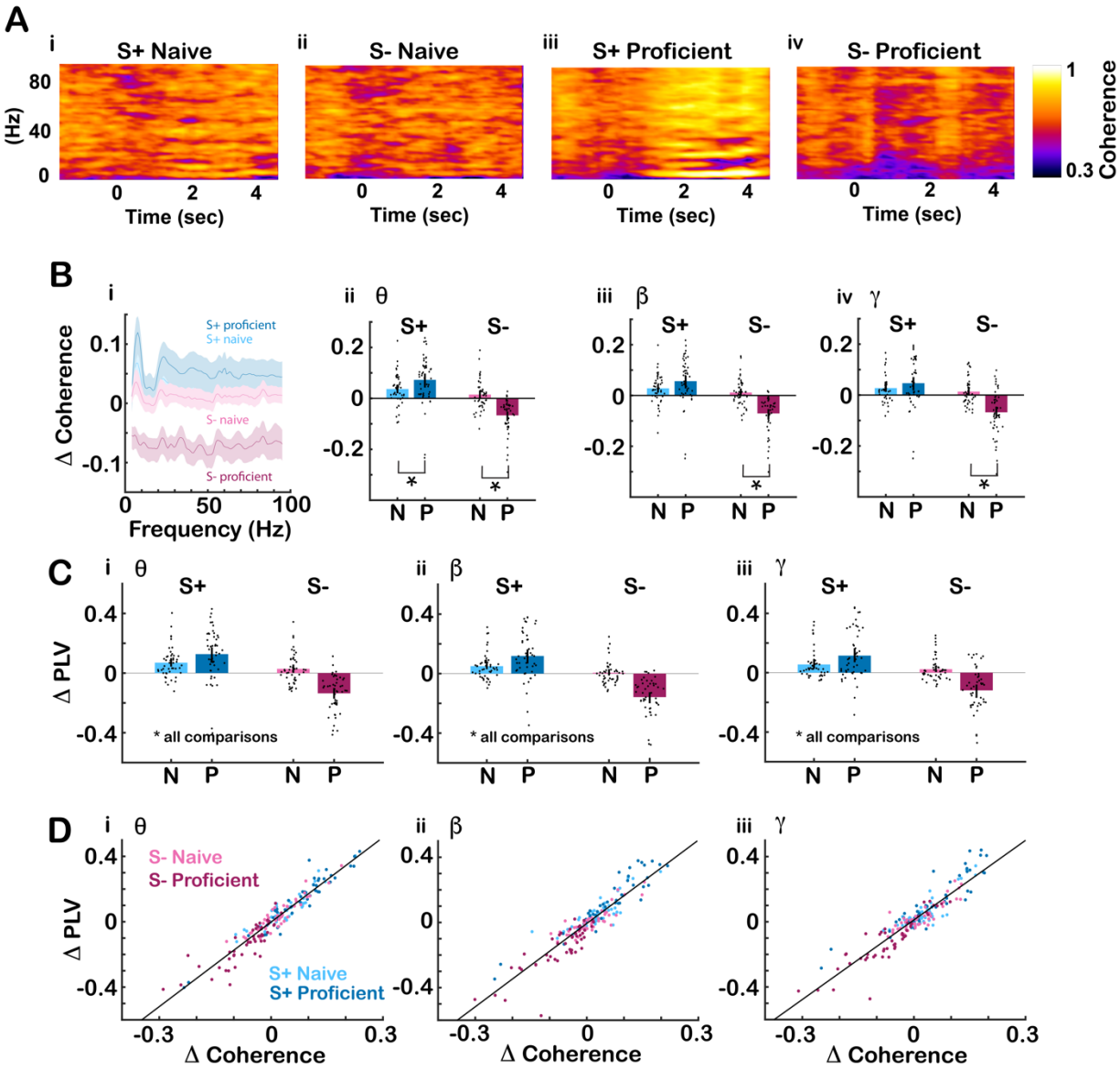

Figure 5. Odorant-elicited change in coherence and phase locking value decreased for the unrewarded odorant as the animal became proficient.

A. Example of pseudocolor plots of the average coherence time course per trial for (i) S+ naïve (30 trials) (ii) S- naïve (27 trials) (iii) S+ proficient (84 trials) (iv) S- proficient (84 trials). B. Summary for Δ coherence as the animal learns. (i) Frequency dependence for the average Δ coherence per mouse per odor pair elicited by the odorant for S+ naïve, S- naïve, S+ proficient and S- proficient (6 mice, 8 odor pairs, the bounded line

830 is the 95% CI). (ii to v) Average Δ coherence elicited by the odorant for the different
831 bandwidths (per mouse per odorant pair): (ii) theta, (iii) beta, (iv) gamma (6 mice, 8 odor
832 pairs, the vertical line is the 95% CI). Δ coherence decreases for S- as the animal
833 becomes proficient. GLM finds statistically significant differences for S+ vs. S- and the
834 interaction between S+ vs. S- and naïve vs. proficient ($p<0.001$, 190 observations, 186
835 d.f., F-statistic=21.6-32.4, $p<0.001$, 6 mice, 8 odor pairs, Supplementary Table 6). C.
836 Bar graphs showing odor-elicited change in average odorant-elicited change in Δ PLV
837 per mouse per odor pair for (i) theta, (ii) beta, (iii) gamma. (6 mice, 8 odor pairs, the
838 vertical line is the 95% CI). GLM finds statistically significant differences between naïve
839 vs. proficient ($p<0.05$) and for S+ vs. S- and the interaction between S+ vs. S- and
840 naïve vs. proficient ($p<0.001$, 192 observations, 188 d.f., F-statistic=29.5-46.5, $p<0.001$,
841 6 mice, 8 odor pairs, Supplementary Table 7). D. Correlation between the odor-elicited
842 change in coherence and the change in Δ PLV for (i) theta, (ii) beta, (iii) gamma. This
843 shows a relationship between Δ coherence and Δ PLV (correlation coefficient > 0.91,
844 $p<0.001$).
845

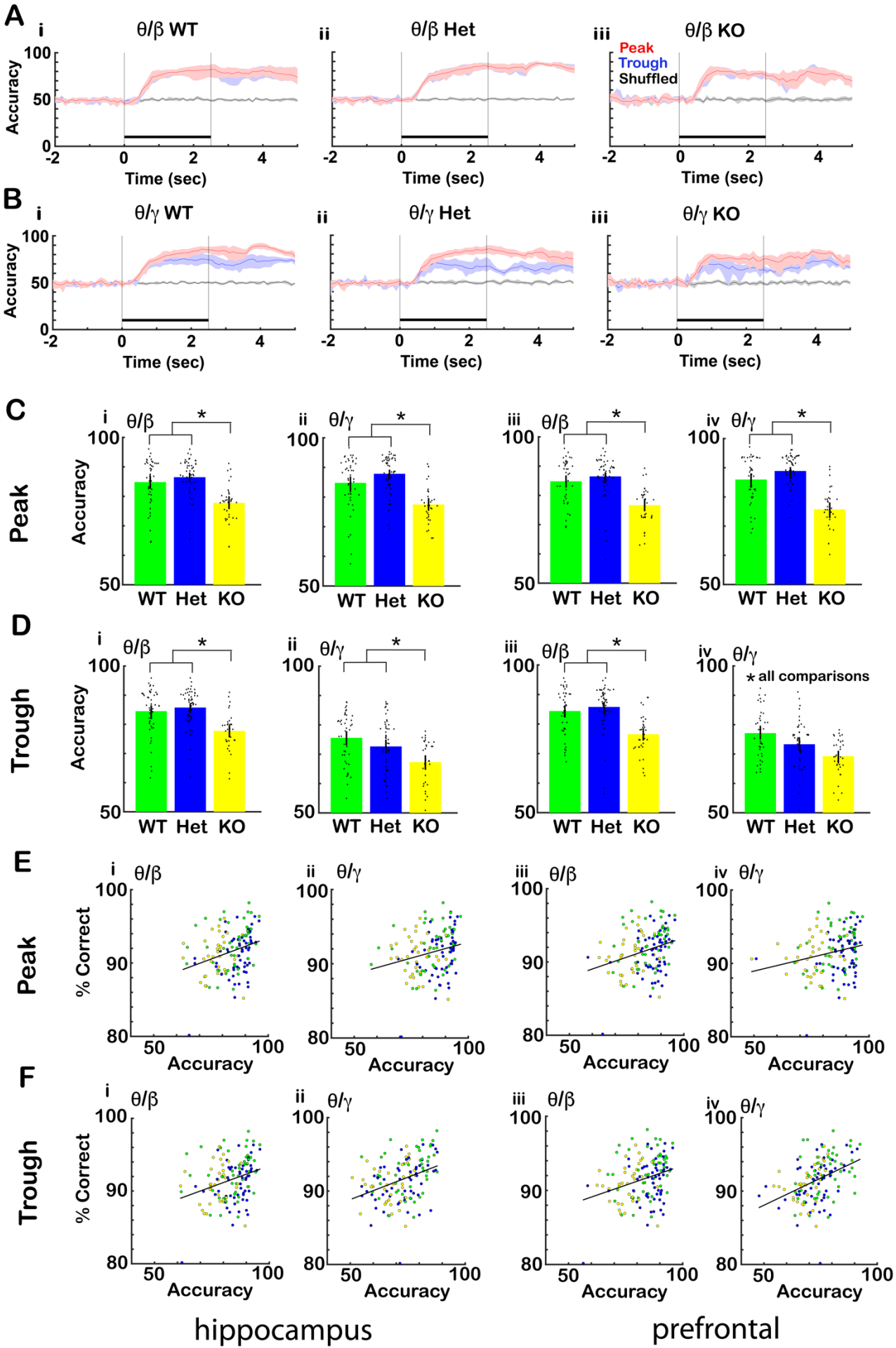
A
i θ/β WT
ii θ/β Het
iii θ/β KO
Peak
Trough
Shuffled
Accuracy
Time (sec)
B
i θ/γ WT
ii θ/γ Het
iii θ/γ KO
C
Peak
i θ/β
ii θ/γ
iii θ/β
iv θ/γ
WT Het KO
D
Trough
* all comparisons
E
Peak
% Correct
Accuracy
F
Trough
hippocampus
prefrontal

847 **Figure 6. The accuracy for decoding the contextual identity of the odorant from**
848 **tPRP decreased in the CaMKIIα knockout mouse and was correlated with percent**
849 **correct discrimination.** A and B. Examples for one mouse of the time course for the
850 accuracy of odorant identification by linear discriminant analysis trained using tPRP for
851 the EAPA odor pair. A. theta/beta PRP. B. theta/gamma PRP. (i) WT, (ii) Het, (iii) KO.
852 Shadow: confidence interval, black bar: odorant application. C and D. Bar graphs
853 showing the differences in discriminant accuracy between the different genotypes. C:
854 Accuracy for peak tPRP for (i) theta/beta in the hippocampus, (ii) theta/gamma in the
855 hippocampus, (iii) theta/beta in mPFC, (iv) theta/gamma in mPFC. D: Accuracy for
856 through for (i) theta/beta in the hippocampus, (ii) theta/gamma in the hippocampus, (iii)
857 theta/beta in mPFC, (iv) theta/gamma mPFC. The bars show the average accuracy, and
858 the points are the accuracy per mouse per odor pair. The vertical bars show the
859 confidence interval. For beta tPRP LDA GLM finds statistically significant differences
860 between WT and KO for all conditions ($p<0.001$) and between WT and Het for
861 theta/gamma trough PRP ($p<0.05$, 756 observations, 744 d.f., F-statistic=9.9-34.3,
862 $p<0.001$, 6 mice, 8 odor pairs, Supplementary Table 11). Asterisks show significant p
863 values ($p<pFDR$) for post-hoc pairwise tests. E. Relationship for proficient mice between
864 percent correct in the go-no go behavior and accuracy of odor identification by the LDA
865 decoding algorithm shown per mouse per odor pair (6 mice, 8 odor pairs). The
866 correlation coefficients were: E (i) 0.3, E (ii) 0.24, E (iii) 0.29, E (iv) 0.23, F (i) 0.3, F (ii)
867 0.36, F (iii) 0.29, F (iv) 0.40, and the p value for significance was $p<0.01$. Lines are best
868 fit lines.
869

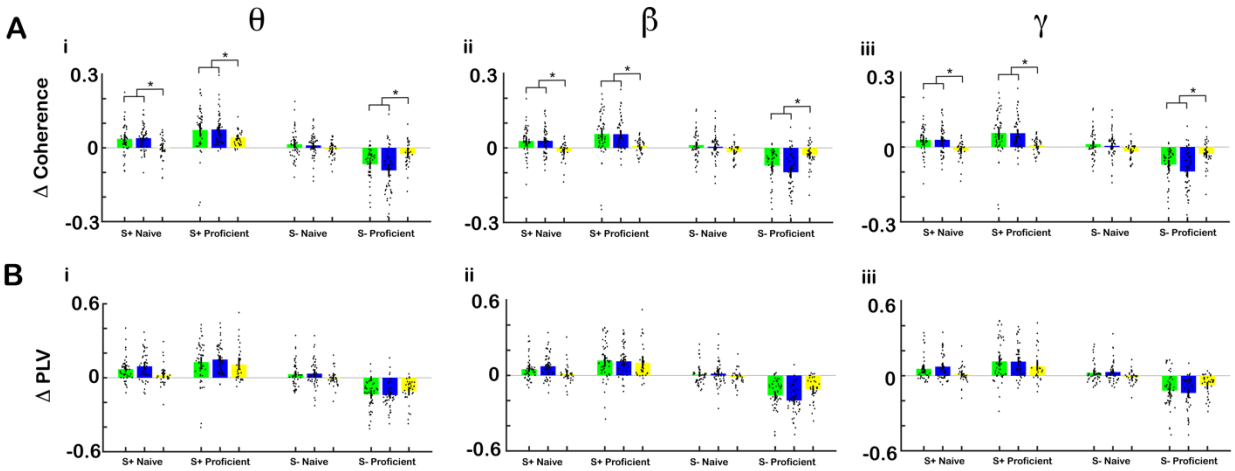

Figure 7. The odorant-elicited change in coherence was smaller for CaMKIIα knockout mice.

A. Summary bar graphs comparing the odorant-elicited change in coherence (Δ coherence) for the different genotypes. (i) theta, (ii) beta, (iii) gamma. The bars show the average Δ coherence, and the points are Δ coherence per mouse per odor pair. The vertical bars show the confidence interval. For Δ coherence GLM finds statistically significant differences between WT and KO, and for the interaction of WT vs. KO and S+ vs. S- ($p<0.05$, 546 observations, 534 d.f., F-statistic=21.2-33.8, $p<0.001$, 6 mice, 8 odor pairs, Supplementary Table 12). Asterisks show significant p values ($p<pFDR$) for post-hoc pairwise tests. B. Summary bar graphs comparing change in Δ PLV for the different genotypes. (i) beta, (ii) theta, (iii) gamma. For Δ PLV GLM finds no statistically significant differences between WT and KO, and for the interaction of WT vs. KO and S+ vs. S- ($p>0.05$, 512 observations, 500 d.f., F-statistic=25.5-39.9, $p<0.001$, 6 mice, 8 odor pairs, Supplementary Table 13).

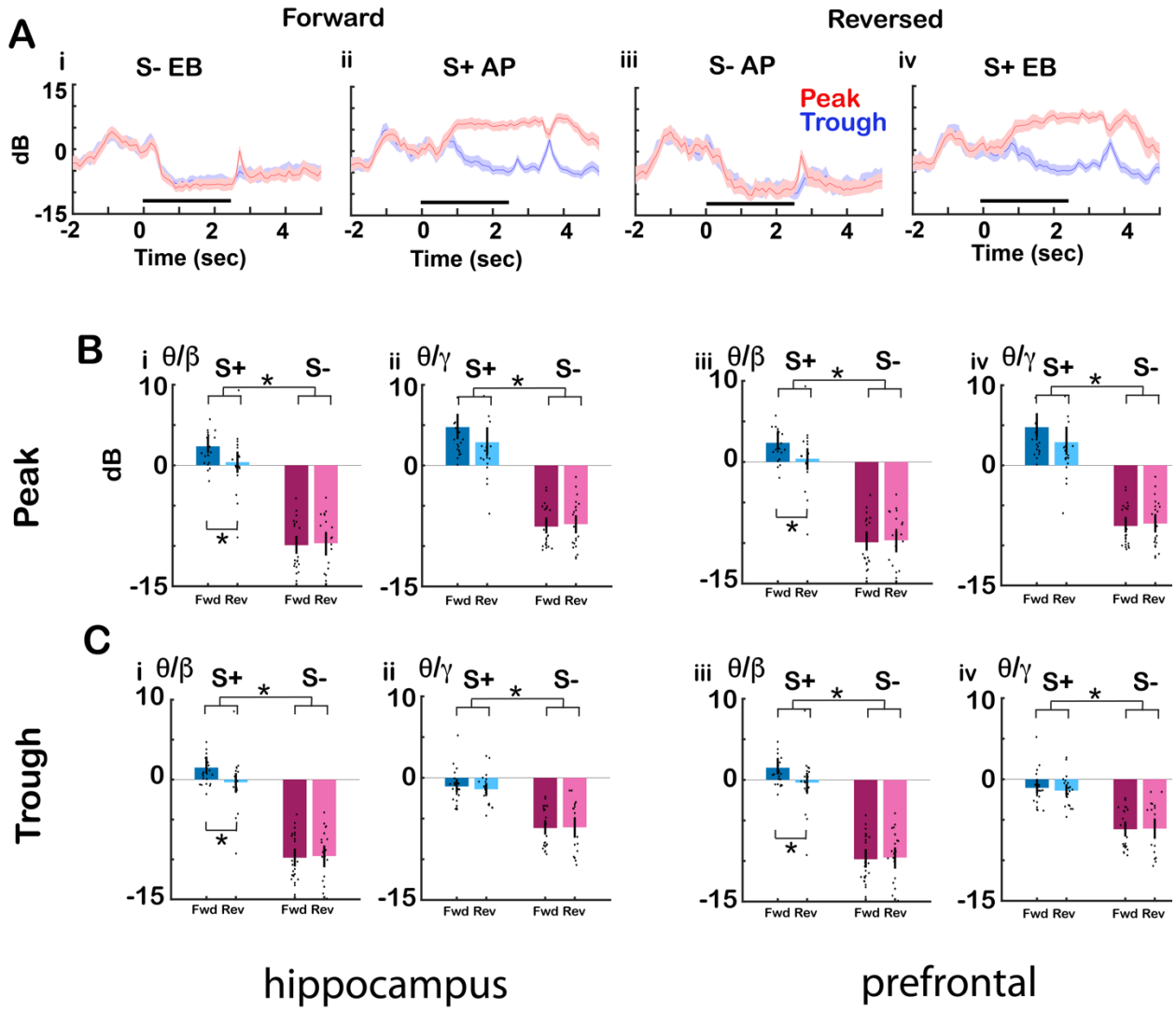

Figure 3 – Figure Supplement 1. Effect of reversal of odorant valence on the phase referenced power. (A) Average gamma wavelet power referenced to theta peak and through for the same trials when the mouse was proficient shown in Figure 3A. The gamma tPRP is normalized by subtracting the power before odorant application. (i,ii) Forward: (i) S- (ethyl benzoate, EB) (ii) S+ (acetophenone, AP); (iii,iv) Reversed: (iii) S- (acetophenone, AP) (iv) S+ (ethyl benzoate, EB), red: peak, blue: through, shadow; confidence interval. (B,C) Summary bar graphs showing that the average peak tPRP decreases for S- upon odorant application regardless of the identity of the odorant. B:

peak, C: through, (i) theta/beta and (ii) theta/gamma hippocampus (iii) theta/beta and (iv) theta/gamma prefrontal cortex. For beta tPRP GLM finds statistically significant differences for forward vs. reverse ($p<0.05$) and S+ vs. S- ($p<0.001$, 188 observations, 180 d.f., F-statistic=87, $p<0.001$, 6 mice, 8 odor pairs, Table S12). For gamma tPRP GLM finds statistically significant differences for S+ vs. S- and peak vs. trough ($p<0.001$, 188 observations, 180 d.f., F-statistic=61.8, $p<0.001$, 6 mice, 8 odor pairs, Table S12). Asterisks show significant p values ($p<pFDR$) for post-hoc pairwise tests.

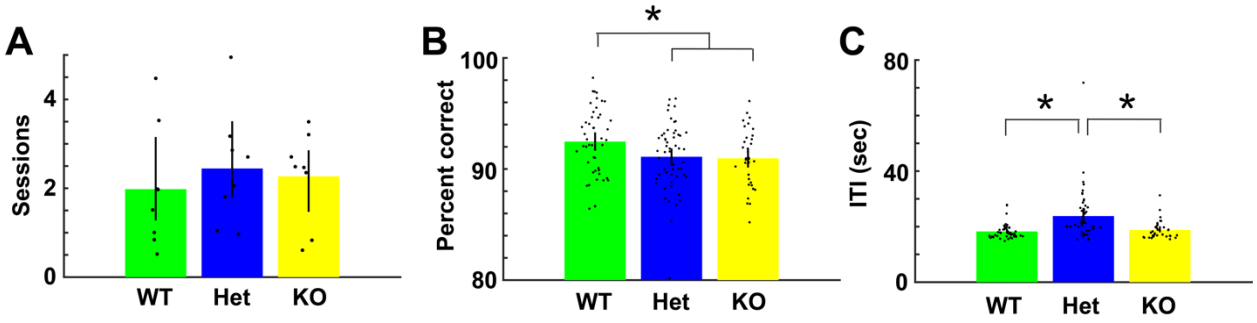

Figure 6 – Figure Supplement 1. Analysis of the behavioral performance for mice of the three genotypes. (A). Number of sessions to criterion per odorant pair (2 blocks of 20 trials with performance >80%). There was no difference between genotypes in the number of sessions to criterion (GLM $p>0.05$, 24 observations, 21 d.f., F-statistic=0.26, $p>0.05$, 8 odor pairs). (B) Percent correct for proficient mice per odorant per mouse. GLM finds a statistical difference for WT compared to both CaMKIIα Het and CaMKIIα KO (GLM $p<0.05$, 137 observations, 134 d.f., F-statistic=3.7, $p<0.05$, 6 mice, 8 odor pairs). (C). Intertrial interval (ITI) for proficient mice. GLM analysis finds that the ITI for CaMKIIα Het differed from both CaMKIIα Het and CaMKIIα KO ($p<0.001$, 137 observations, 134 d.f., F-statistic=13.5, $p<0.001$, 6 mice, 8 odor pairs). Asterisks denote statistically significant differences evaluated with either t test or ranksum corrected for multiple comparisons ($p<pFDR$).

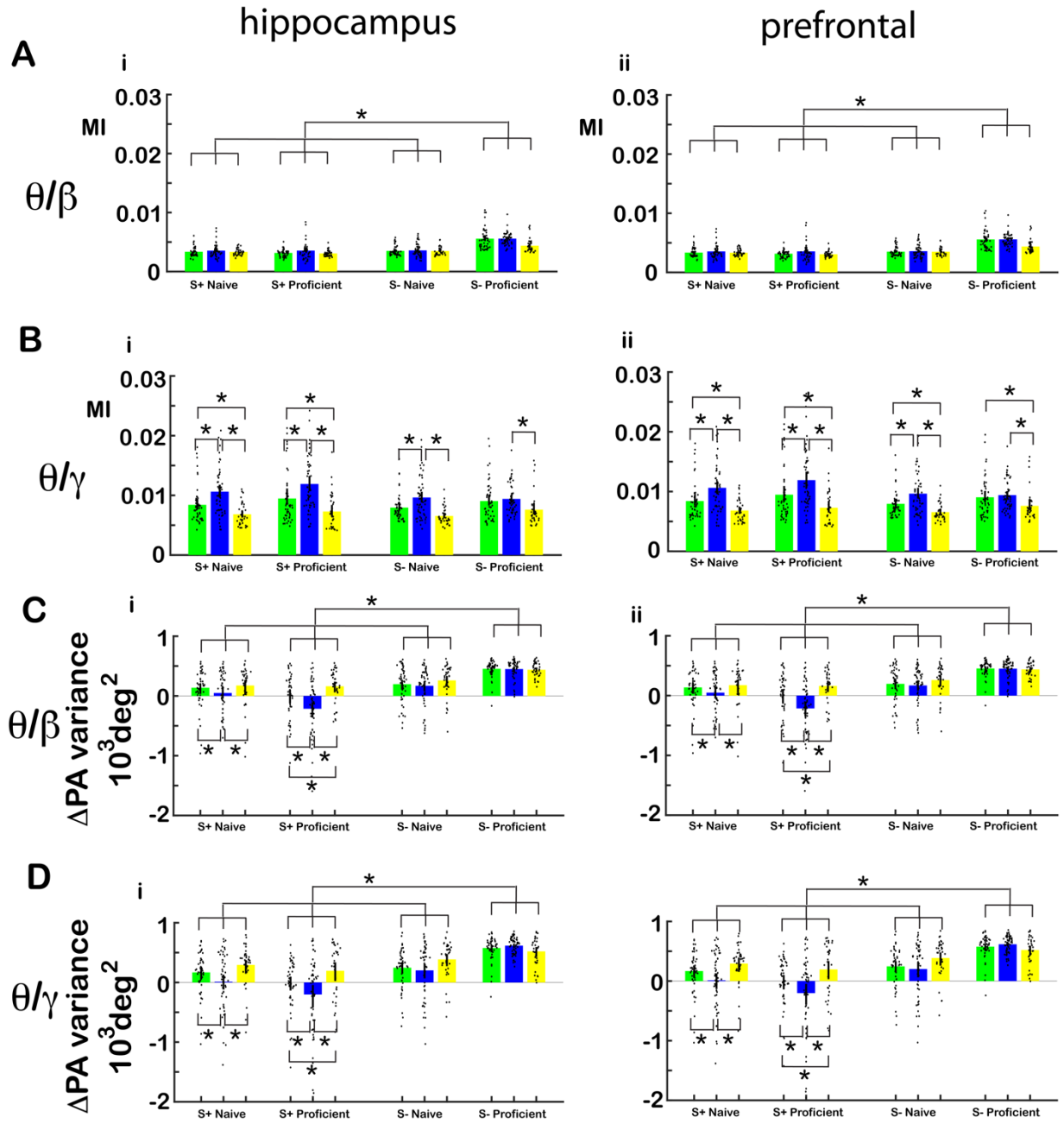

Figure 6 – Figure Supplement 2. PAC and peak angle variance per genotype

(A,B) Bar graphs showing average MI per mouse per odor pair for each genotype, S+ and S- in naïve and proficient mice for (A) theta/beta and (B) theta/gamma for (i) hippocampus and (ii) mPFC. The bars show the average MI, and the points are the MI per mouse per odor pair. For theta/beta PAC MI GLM finds a statistically significant

927 difference for S+ vs. S-, for the interaction of WT vs. KO and S+ vs. S- and the
928 interaction of WT vs. KO and naïve vs. proficient ($p<0.001$, 544 observations, 532 d.f.,
929 F-statistic=10.3-34.3, $p<0.001$, 6 mice, 8 odor pairs, Table S10). For theta/gamma PAC
930 MI GLM finds a statistically significant difference between WT vs. KO and WT vs. Het
931 ($p<0.01$) and for the interaction of WT vs. Het and S+ vs. S- ($p<0.05$, 544 observations,
932 532 d.f., F-statistic=10.3-34.3, $p<0.001$, 6 mice, 8 odor pairs, Table S10). (C,E) Bar
933 graphs showing average peak angle variance per mouse per odor pair for each
934 genotype, S+ and S- in naïve and proficient mice for (A) theta/beta and (B)
935 theta/gamma for (i) hippocampus and (ii) mPFC. For theta/beta PAC MI GLM finds a
936 statistically significant difference for WT vs. Het ($p<0.001$) and WT vs. KO ($p<0.05$), S+
937 vs. S-, ($p<0.001$) and naïve vs. proficient ($p<0.05$, 544 observations, 532 d.f., F-
938 statistic=20.6, $p<0.001$, 6 mice, 8 odor pairs, Table S11). For theta/gamma PAC MI
939 GLM finds a statistically significant difference for WT vs. Het ($p<0.05$) and WT vs. KO
940 ($p<0.05$), S+ vs. S-, ($p<0.001$) and naïve vs. proficient ($p<0.05$, 544 observations, 532
941 d.f., F-statistic=18.8, $p<0.001$, 6 mice, 8 odor pairs, Table S11).
942
943

Note: Supplementary tables show the output of the MATLAB code that performs the GLM analysis and the pairwise ranksum/t test. They will be included in our resubmission.

References

Agresti, A. (2015). Foundations of linear and generalized linear models. In Wiley series in probability and statistics (Hoboken, New Jersey: John Wiley & Sons Inc.,), pp. 1 online resource.

Bayer, K.U., and Schulman, H. (2019). CaM Kinase: Still Inspiring at 40. Neuron *103*, 380-394.

Bear, M.F., Cooke, S.F., Giese, K.P., Kaang, B.K., Kennedy, M.B., Kim, J.I., Morris, R.G.M., and Park, P. (2018). In memoriam: John Lisman - commentaries on CaMKII as a memory molecule. Mol Brain *11*, 76.

Belluscio, M.A., Mizuseki, K., Schmidt, R., Kempter, R., and Buzsáki, G. (2012). Cross-Frequency Phase–Phase Coupling between Theta and Gamma Oscillations in the Hippocampus. The Journal of Neuroscience *32*, 423.

Bliss, T.V., and Lomo, T. (1973). Long-lasting potentiation of synaptic transmission in the dentate area of the anaesthetized rabbit following stimulation of the perforant path. J Physiol *232*, 331-356.

Borjigin, J., Lee, U., Liu, T., Pal, D., Huff, S., Klarr, D., Sloboda, J., Hernandez, J., Wang, M.M., and Mashour, G.A. (2013). Surge of neurophysiological coherence and connectivity in the dying brain. Proceedings of the National Academy of Sciences *110*, 14432.

Buonviso, N., Amat, C., Litaudon, P., Roux, S., Royet, J.P., Farget, V., and Sicard, G. (2003). Rhythm sequence through the olfactory bulb layers during the time window of a respiratory cycle. EurJNeurosci *17*, 1811-1819.

Butler, J.L., Mendonça, P.R.F., Robinson, H.P.C., and Paulsen, O. (2016). Intrinsic Cornu Ammonis Area 1 Theta-Nested Gamma Oscillations Induced by Optogenetic Theta Frequency Stimulation. The Journal of Neuroscience *36*, 4155.

Cajal, S. (1904). Textura del sistema nervioso del hombre y de los vertebrados (Madrid: Moya).

Cansler, H.L., in ’t Zandt, E.E., Carlson, K.S., Khan, W.T., Ma, M., and Wesson, D.W. (2021). Organization and engagement of a prefrontal-olfactory network during olfactory selective attention. bioRxiv, 2021.2009.2004.458996.

Chen, C., Rainnie, D.G., Greene, R.W., and Tonegawa, S. (1994). Abnormal fear response and aggressive behavior in mutant mice deficient for alpha-calcium-calmodulin kinase II. Science *266*, 291-294.

Chia, P.H., Zhong, F.L., Niwa, S., Bonnard, C., Utami, K.H., Zeng, R., Lee, H., Eskin, A., Nelson, S.F., Xie, W.H.*, et al.* (2018). A homozygous loss-of-function CAMK2A mutation causes growth delay, frequent seizures and severe intellectual disability. eLife *7*, e32451.

990 Colgin, L.L. (2011). Oscillations and hippocampal–prefrontal synchrony. Current
991 Opinion in Neurobiology *21*, 467-474.

992 Colgin, L.L. (2015). Theta-gamma coupling in the entorhinal-hippocampal system. Curr
993 Opin Neurobiol *31*, 45-50.

994 Cook, S.G., Buonarati, O.R., Coultrap, S.J., and Bayer, K.U. (2021). CaMKII
995 holoenzyme mechanisms that govern the LTP versus LTD decision. Sci Adv *7*.

996 Coultrap, S.J., Freund, R.K., O'Leary, H., Sanderson, J.L., Roche, K.W., Dell'Acqua,
997 M.L., and Bayer, K.U. (2014). Autonomous CaMKII mediates both LTP and LTD using a
998 mechanism for differential substrate site selection. Cell Rep *6*, 431-437.

999 Curran-Everett, D. (2000). Multiple comparisons: philosophies and illustrations.
1000 AmJPhysiol RegulIntegrComp Physiol *279*, R1-R8.

1001 Eleore, L., Lopez-Ramos, J.C., Guerra-Narbona, R., and Delgado-Garcia, J.M. (2011).
1002 Role of reuniens nucleus projections to the medial prefrontal cortex and to the
1003 hippocampal pyramidal CA1 area in associative learning. PLoS One *6*, e23538.

1004 Frankland, P.W., O'Brien, C., Ohno, M., Kirkwood, A., and Silva, A.J. (2001). Alpha-
1005 CaMKII-dependent plasticity in the cortex is required for permanent memory. Nature
1006 *411*, 309-313.

1007 Fries, P. (2005). A mechanism for cognitive dynamics: neuronal communication through
1008 neuronal coherence. Trends Cogn Sci *9*, 474-480.

1009 Fromer, M., Pocklington, A.J., Kavanagh, D.H., Williams, H.J., Dwyer, S., Gormley, P.,
1010 Georgieva, L., Rees, E., Palta, P., Ruderfer, D.M.*, et al.* (2014). De novo mutations in
1011 schizophrenia implicate synaptic networks. Nature *506*, 179-184.

1012 Goodell, D.J., Benke, T.A., and Bayer, K.U. (2016). Developmental restoration of LTP
1013 deficits in heterozygous CaMKIIα KO mice. Journal of Neurophysiology *116*, 2140-2151.

1014 Gordon, J.A. (2011). Oscillations and hippocampal–prefrontal synchrony. Current
1015 Opinion in Neurobiology *21*, 486-491.

1016 Gourevitch, B., Kay, L.M., and Martin, C. (2010). Directional coupling from the olfactory
1017 bulb to the hippocampus during a go/no-go odor discrimination task. J Neurophysiol
1018 *103*, 2633-2641.

1019 Halsey, L.G., Curran-Everett, D., Vowler, S.L., and Drummond, G.B. (2015). The fickle
1020 P value generates irreproducible results. Nature methods *12*, 179-185.

1021 Hasegawa, S., Furuichi, T., Yoshida, T., Endoh, K., Kato, K., Sado, M., Maeda, R.,
1022 Kitamoto, A., Miyao, T., Suzuki, R.*, et al.* (2009). Transgenic up-regulation of alpha-
1023 CaMKII in forebrain leads to increased anxiety-like behaviors and aggression. Mol Brain
1024 *2*, 6.

Headley, D.B., and Paré, D. (2017). Common oscillatory mechanisms across multiple memory systems. npj Science of Learning *2*, 1.

Kaplan, R., Bush, D., Bonnefond, M., Bandettini, P.A., Barnes, G.R., Doeller, C.F., and Burgess, N. (2014). Medial prefrontal theta phase coupling during spatial memory retrieval. Hippocampus *24*, 656-665.

Klein, S.B., Cosmides, L., Tooby, J., and Chance, S. (2002). Decisions and the evolution of memory: multiple systems, multiple functions. Psychol Rev *109*, 306-329.

Lachaux, J.P., Rodriguez, E., Martinerie, J., and Varela, F.J. (1999). Measuring phase synchrony in brain signals. Hum Brain Mapp *8*, 194-208.

Larson, J., and Munkácsy, E. (2015). Theta-burst LTP. Brain Research *1621*, 38-50.

Li, A., Gire, D.H., and Restrepo, D. (2015). Y spike-field coherence in a population of olfactory bulb neurons differentiates between odors irrespective of associated outcome. J Neurosci *35*, 5808-5822.

Li, Y., Xu, J., Liu, Y., Zhu, J., Liu, N., Zeng, W., Huang, N., Rasch, M.J., Jiang, H., Gu, X.*, et al.* (2017). A distinct entorhinal cortex to hippocampal CA1 direct circuit for olfactory associative learning. Nature Neuroscience *20*, 559-570.

1041 Lisman, J., Buzsaki, G., Eichenbaum, H., Nadel, L., Ranganath, C., and Redish, A.D.
1042 (2017). Viewpoints: how the hippocampus contributes to memory, navigation and
1043 cognition. Nat Neurosci *20*, 1434-1447.

1044 Lisman, J., Yasuda, R., and Raghavachari, S. (2012). Mechanisms of CaMKII action in
1045 long-term potentiation. Nat Rev Neurosci *13*, 169-182.

1046 Losacco, J., Ramirez-Gordillo, D., Gilmer, J., and Restrepo, D. (2020). Learning
1047 improves decoding of odor identity with phase-referenced oscillations in the olfactory
1048 bulb. Elife *9*, e52583.

1049 Malinow, R., Schulman, H., and Tsien Richard, W. (1989). Inhibition of Postsynaptic
1050 PKC or CaMKII Blocks Induction But Not Expression of LTP. Science *245*, 862-866.

1051 Malvaut, S., Gribaudo, S., Hardy, D., David, L.S., Daroles, L., Labrecque, S., Lebel-
1052 Cormier, M.-A., Chaker, Z., Coté, D., De Koninck, P.*, et al.* (2017). CaMKIIalpha
1053 Expression Defines Two Functionally Distinct Populations of Granule Cells Involved in
1054 Different Types of Odor Behavior. Current Biology *27*, 3315-3329.e3316.

1055 Martin, C., Beshel, J., and Kay, L.M. (2007). An olfacto-hippocampal network is
1056 dynamically involved in odor-discrimination learning. JNeurophysiol *98*, 2196-2205.

Matsuo, N., Yamasaki, N., Ohira, K., Takao, K., Toyama, K., Eguchi, M., Yamaguchi, S., and Miyakawa, T. (2009). Neural activity changes underlying the working memory deficit in alpha-CaMKII heterozygous knockout mice. Front Behav Neurosci *3*, 20.

Moberly, A.H., Schreck, M., Bhattarai, J.P., Zweifel, L.S., Luo, W., and Ma, M. (2018). Olfactory inputs modulate respiration-related rhythmic activity in the prefrontal cortex and freezing behavior. Nature Communications *9*, 1528.

Mofleh, R., and Kocsis, B. (2021). Delta-range coupling between prefrontal cortex and hippocampus supported by respiratory rhythmic input from the olfactory bulb in freely behaving rats. Scientific Reports *11*, 8100.

Nakazawa, K., McHugh, T.J., Wilson, M.A., and Tonegawa, S. (2004). NMDA receptors, place cells and hippocampal spatial memory. Nature Reviews Neuroscience *5*, 361-372.

Namburi, P. (2021). Phase locking value. https://praneethnamburi.com/2011/08/10/plv/.

Nguyen Chi, V., Muller, C., Wolfenstetter, T., Yanovsky, Y., Draguhn, A., Tort, A.B., and Brankack, J. (2016). Hippocampal Respiration-Driven Rhythm Distinct from Theta Oscillations in Awake Mice. J Neurosci *36*, 162-177.

Purcell, S.M., Moran, J.L., Fromer, M., Ruderfer, D., Solovieff, N., Roussos, P., O'Dushlaine, C., Chambert, K., Bergen, S.E., Kahler, A.*, et al.* (2014). A polygenic burden of rare disruptive mutations in schizophrenia. Nature *506*, 185-190.

1075 Robison, A.J. (2014). Emerging role of CaMKII in neuropsychiatric disease. Trends in
1076 Neurosciences *37*, 653-662.

1077 Rojas-Libano, D., Frederick, D.E., Egana, J.I., and Kay, L.M. (2014). The olfactory bulb
1078 theta rhythm follows all frequencies of diaphragmatic respiration in the freely behaving
1079 rat. Front Behav Neurosci *8*, 214.

1080 Scheffer-Teixeira, R., and Tort, A.B. (2016). On cross-frequency phase-phase coupling
1081 between theta and gamma oscillations in the hippocampus. eLife *5*, e20515.

1082 Siegle, J.H., and Wilson, M.A. (2014). Enhancement of encoding and retrieval functions
1083 through theta phase-specific manipulation of hippocampus. Elife *3*, e03061.

1084 Silva, A.J., Paylor, R., Wehner, J.M., and Tonegawa, S. (1992a). Impaired spatial
1085 learning in alpha-calcium-calmodulin kinase II mutant mice. Science *257*, 206-211.

1086 Silva, A.J., Rosahl, T.W., Chapman, P.F., Marowitz, Z., Friedman, E., Frankland, P.W.,
1087 Cestari, V., Cioffi, D., Südhof, T.C., and Bourtchuladze, R. (1996). Impaired learning in
1088 mice with abnormal short-lived plasticity. Current Biology *6*, 1509-1518.

1089 Silva, A.J., Stevens, C.F., Tonegawa, S., and Wang, Y. (1992b). Deficient hippocampal
1090 long-term potentiation in alpha-calcium-calmodulin kinase II mutant mice. Science *257*,
1091 201-206.

1092 Slotnick, B.M., and Restrepo, D. (2005). Olfactometry with mice. In Current Protocols in
1093 Neuroscience, J.N. Crawley, C.R. Gerefen, M.A. Rogawski, D.R. Sibley, P. Skolnick,
1094 and S. Wray, eds. (New York: John Wiley and Sons, Inc), pp. 1-24
1095

1096 Suarez-Pereira, I., Canals, S., and Carrion, A.M. (2015). Adult newborn neurons are
1097 involved in learning acquisition and long-term memory formation: the distinct demands
1098 on temporal neurogenesis of different cognitive tasks. Hippocampus *25*, 51-61.

1099 Tort, A.B., Komorowski, R., Eichenbaum, H., and Kopell, N. (2010). Measuring phase-
1100 amplitude coupling between neuronal oscillations of different frequencies. J
1101 Neurophysiol *104*, 1195-1210.

1102 Udakis, M., Pedrosa, V., Chamberlain, S.E.L., Clopath, C., and Mellor, J.R. (2020).
1103 Interneuron-specific plasticity at parvalbumin and somatostatin inhibitory synapses onto
1104 CA1 pyramidal neurons shapes hippocampal output. Nature Communications *11*, 4395.

1105 Vizcay, M.A., Duarte-Mermoud, M.A., and Aylwin Mde, L. (2015). Odorant recognition
1106 using biological responses recorded in olfactory bulb of rats. Comput Biol Med *56*, 192-
1107 199.

1108 Walton, N.M., Zhou, Y., Kogan, J.H., Shin, R., Webster, M., Gross, A.K., Heusner, C.L.,
1109 Chen, Q., Miyake, S., Tajinda, K.*, et al.* (2012). Detection of an immature dentate gyrus
1110 feature in human schizophrenia/bipolar patients. Transl Psychiatry *2*, e135.

1111 Won, G.H., Kim, J.W., Choi, T.Y., Lee, Y.S., Min, K.J., and Seol, K.H. (2018). Theta-
1112 phase gamma-amplitude coupling as a neurophysiological marker in neuroleptic-naïve
1113 schizophrenia. Psychiatry Research *260*, 406-411.

1114 Yamasaki, N., Maekawa, M., Kobayashi, K., Kajii, Y., Maeda, J., Soma, M., Takao, K.,
1115 Tanda, K., Ohira, K., Toyama, K.*, et al.* (2008). Alpha-CaMKII deficiency causes
1116 immature dentate gyrus, a novel candidate endophenotype of psychiatric disorders.
1117 Molecular Brain *1*, 6.
1118